ABSTRACT

JET ASSISTED FLUIDIZATION
OF NANOPARTICLE AGGLOMERATES

by
Ayokunle O. Omosebi

Fluidization serves as a primary operation used to disperse, handle and process nanoparticles, but due to the complications involved with achieving homogenous fluidization of the agglomerates of nanoparticles, several methods have been developed to assist their conventional mode of fluidization.

In this work, the conventional mode of fluidization was coupled with secondary gas flow emerging from a micro jet nozzle. The effect of the jet on the fluidization behavior of various APF and ABF nanopowders was studied and compared with the pure conventional fluidization mode. Generally, experiments were conducted to find the optimal operation of the jet by varying parameters such as, nozzle size, nozzle pressure, number of nozzles, orientation, position of nozzle, and the amount of powder affected by the nozzle.

It was found that under the influence of the jet, better dispersion of the bed of nanoparticle agglomerates was achieved, and this was true for the different powders that were used under different operating conditions. Besides improved dispersion, it was also found that the jet served to break down the larger agglomerates, to reduce the minimum fluidization velocity, to delay the onset of bubbling, and to convert the fluidization behavior of ABF powder to APF.

JET ASSISTED FLUIDIZATION
OF NANOPARTICLE AGGLOMERATES

by
Ayokunle O. Omosebi

A Thesis
Submitted to the Faculty of
New Jersey Institute of Technology
in Partial Fulfillment of the Requirements for the Degree of
Master of Science in Chemical Engineering

Otto York Department of Chemical Engineering

January 2007

Blank Page

APPROVAL PAGE

JET ASSISTED FLUIDIZATION
OF NANOPARTICLE AGGLOMERATES

Ayokunle O. Omosebi

Dr. Robert Pfeffer, Thesis Advisor   Date
Distinguished Professor, Dept of Chemical Engineering, NJIT

Dr. Norman Loney, Committee Member   Date
Associate Professor, Dept of Chemical Engineering, NJIT

Dr. Jing Wu, Committee Member   Date
Assistant Professor, Dept of Chemical Engineering, NJIT

BIOGRAPHICAL SKETCH

Author: Ayokunle O. Omosebi

Degree: Master of Science

Date: January 2007

Undergraduate and Graduate Education:

- Master of Science in Chemical Engineering,
  New Jersey Institute of Technology, Newark, NJ, 2007

- Bachelor of Science in Chemical Engineering,
  City College, City University of New York, New York NY, 2004

Major: Chemical Engineering

Publications:

Daniel Lepek, Jose Quevedo, Ayokunle Omosebi, Rajesh Dave, Robert Pfeffer
    The Effect of Gas Viscosity on the Agglomerate Particulate Fluidization State of
    Fine and Ultrafine Particles, *in preparation*

Jose A. Quevedo, Ayokunle Omosebi, Robert Pfeffer
    Enhancement of Gas-Solid fluidization of Agglomerates of fumed Metal Oxide
    Nanoparticles, *in preparation*

To my parents
Bukola and Adebayo

ACKNOWLEDGMENT

TABLE OF CONTENTS

LIST OF TABLES

LIST OF FIGURES

x

LIST OF SYMBOLS

Ar	Archimedes number, dimensionless
A_t	Transversal area of the fluidization column, m^2
C_D	Drag coefficient, dimensionless
d_p	Diameter of particle, m
d_o	Nozzle diameter, m
D_b	Bubble diameter, m
F	Force, N
F_b	Buoyancy force, N
F_c	Cohesive force, N
F_d	Drag force, N
F_g	Gravitational force, N
Fr	Froude Number
g	Gravitational acceleration, m/s^2 (9.8)
g_c	Conversion factor, 1 $N.s^2/(kg.m)$
G	Gravitational factor, dimensionless
H	Fluidized bed height, cm
H_0	Initial bed height at no flow, cm
k_1	Energy cohesive constant, J/nm

K_1	Constant, dimensionless
K_2	Constant, dimensionless
K_3	Constant in Equation
N	Number of particles per unit volume, $1/m^3$
n	Richardson & Zaki index, dimensionless
L_m	Length of the bed expansion, m
L_{mf}	Length of the bed expansion at minimum fluidization, m
L_j	Jet Penetration depth
P	Pressure, Pa
P_O	Pressure at the beginning of the channel, Pa
P_L	Pressure at the end of the channel, Pa
Re	Reynolds number, dimensionless
Re_p	Reynolds number based on particle diameter, dimensionless
$Re_{p,mf}$	Reynolds number based on particle diameter at minimum fluidization conditions, dimensionless
St	Stokes number
t	Time, s
u	local fluid velocity, cm/s
u_o	fluid velocity, cm/s
U	Gas velocity, cm/s

U_p	Particle velocity, cm/s
U_j	Jet velocity
U_m	Velocity at axis of the jet
u_g	Fluidization velocity, m/s
u_{mf}	Minimum fluidization velocity, cm/s
U_t	Terminal velocity of the particle, m/s
v_t	Terminal velocity of the particle, m/s
V_B	Particle volume fraction, m
V_p	Volume of particle, m^3
W	Weight of the bed of powder, N

Greek letters

ε	Void fraction or interparticle voidage, dimensionless
ε_m	Void fraction, dimensionless
ε_I	Empty spaces inside the agglomerate of nanoparticles, dimensionless
ε_{mf}	Void fraction at minimum fluidization, dimensionless
μ	Fluid viscosity, (N.s/m^2)
μ_f	Fluid viscosity, (N.s/m^2)
μ_g	Viscosity of the gas, (N.s/m^2)

ρ_a	Density of agglomerate, kg/m^3
ρ_b	Bulk density of the bed of agglomerates, kg/m^3
ρ_f	Gas or fluid density, kg/m^3
ρ_p	Particle density, kg/m^3
ρ_s	Solid particle density, kg/m^3
ϕ	Solids volume fraction, dimensionless
ϕ_s	Sphericity of a particle, dimensionless
Δp	Bed pressure drop, Pa

CHAPTER 1

INTRODUCTION: NANO-FLUIDIZATION AND CONCEPTS ON CONVENTIONAL FLUIDIZATION

1.1 Overview

Fluidization is the suspension of a bed of particles by a fluid. In the fluidized state, the fluid moving through the bed exerts a drag force on the solid phase to balance the weight of the bed of particles, and under the equilibrium of forces, the bed of particles acquires fluid like properties. In other words, the bed will respond to a pressure gradient by flowing. The fluidization process is very desirable and useful, because it represents a regime where high rates of heat and mass transfer, and mixing are possible. As a result, fluidization is applied in gasification processes, heat exchange, particle coating, drying, adsorption, reactions, and many more operations.

Fluidization can be classified based on the nature of the fluid involved, i.e. liquid phase and gas phase fluidization, but there are also operations which make use of both phases. The fluidized bed refers to an equipment setup for the purpose of dispersing a bed of particles. The bed of particles is a powder, whose primary particle size can range from the nano-scale to the milli-scale. For nanometer sized particles, the cohesive forces between the individual primary particles is quite strong, hence they combine together to form larger agglomerates. These fine cohesive nanopowders or nanoparticle agglomerates, as they are termed, tend to be difficult to disperse in the absence of some form of pretreatment or excitation. As a result, a lot of research has been devoted to finding ways to better handle them.

1

For nanoparticle agglomerates, their fluidization behavior has been classified as either Agglomerate particle fluidization (APF) or Agglomerate bubbling fluidization (ABF) (Yao et al. 2002). This classification depends mostly on the bulk density and the primary particle size. APF particles are typified by their high bed expansion, smooth, mostly homogenous, and liquid like behavior, while ABF particles tend to be non-homogenous and bubble aggressively as explained by Yao et al. (2002)

Nanoparticles as mentioned earlier have become the subject of much research and many discussions due to their varied applications and usefulness. Consequently, ways to effectively handle these powders in large quantities has also become very important. Fluidization is primarily used to handle and disperse these particles in large quantities for coating, chemical reactions, adsorption of reactants, and other applications. Agglomerates of nanoparticles are used in the production of paints, gels, printing inks, coatings. etc., but as previously mentioned, due to the cohesive nature of the nanoparticles, they are difficult to homogenously fluidize via conventional methods.

Usually when the fluidization of these nanoparticle agglomerates is attempted, they tend to channel, lift as a plug, elutriate, and bubble. These are not desirable operational qualities because they represent gas bypass and loss of reactant and/or particles. However, improved methods have been suggested by researchers to ensure successful fluidization of these nanoparticles agglomerates. Prominent among them are sound assisted fluidization (Zhu et al. 2004, Guo et al. 2006), vibration assisted fluidization (Nam et al. 2004, Hakim et al. 2005, Levy et al. 2006), the use of the rotational fluidized bed (Quevedo et al. 2006), fluidization in an oscillating magnetic field (Yu et al. 2005), and surface modification (Guo et al. 2006). It should also be noted

that a combination of some of the methods listed is also feasible in some cases (Levy, 2006). In this research, we have conducted experiments on the fluidization of nanoparticle agglomerates using the assistance of a jet generated by a micro nozzle. This work has been done as part of a project funded by Degussa Corporation under the supervision of Dr Robert. Pfeffer, and in coordination with Jose Quevedo.

1.2 Production of Nanoparticles

Nanoparticles are generally particles that are less than several tens of nanometers in primary particle diameter. Due to their optical properties, high catalytic activity, and unusual physical and mechanical properties, these particles are used as additives to improve the properties of various materials. For example, in liquid systems, nanoparticles are added to improve suspension behavior (Jang, 2001).

There are several ways to produce nanoparticles. For example, titanium oxide was produced in the 1960's using wet phase chemistry, but this method generated huge amounts of sulfuric acid waste (Stark et al. 2002). Later in the 1970's, flame technology contributed decisively to the manufacturing of ultra pure silica. Now, with improved understanding of the mechanisms involved in flame synthesis, even nanoparticles of mixed oxides can be synthesized using flame technology (Stark et al. 2002).

The nanopowders used in this work are Aerosil R974, Aeroxide titanium dioxide, Aerosil 90, Alumina C, and Aerosil 200, with primary particle sizes in the range of 12 to 21 nm. They are produced by Degussa Corporation through a pyrogenic process developed for the production of nanoparticles in large quantities (Mangold et al. 1999).

The reaction for this process is:

$$SiCl_4 + O_2 + H_2 \rightarrow SiO_2 + 2HCl \quad \text{(at high temperature)} \tag{1.1}$$
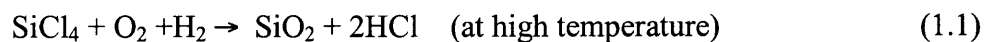
The SiCl$_4$ is vaporized at about $90\,^{\circ}C$, and then mixed with hydrogen and oxygen. The resultant gaseous mixture is then ignited and burned in the combustion chamber of a water cooled flame reactor. The reaction gases are then cooled down, and the pyrogenic silica is filtered from the hydrogen chloride and treated for about 30 seconds at a temperature of 600 $^{\circ}C$ in a de-acidification unit. Generally, the same principle is used in the production of other nanoparticles such as titanium oxide, iron oxide, and alumina oxide (Quevedo, 2004).

It is well known that the fluidization behavior of fine particles is related to the structure and properties of the particles, and nature of the fluid with which it is in contact. Nanoparticles are said to form hierarchical, fractal structured, porous agglomerates, which have very low density and are irregularly shaped (Yao et al. 2002). This feature accounts for their hydrodynamic behavior which differs from that of agglomerates of larger sized particles.

The structure of nanoparticle agglomerates is dependent on geometry, adsorption, electrostatic attraction, and capillarity. It was reported by Yao et al (2002) that the primary particles of SiO$_2$ forms multi-stage agglomerates by several steps with different bonding mechanisms. The building blocks are the nonporous primary nanoparticles which are less than 20 nm that aggregate into netlike porous structures with very low bulk density. Then these netlike porous structures aggregate into simple agglomerates in the range of 1-100 μm, which then combine to form larger more complex agglomerates which may be larger than a millimeter .

1.3 Literature Review

Gas fluidization of fine particles has received significant attention due to its ability to handle the particles. Extensive research has been done on the fluidization of micron sized particles and is generally much better understood compared to the more complex nanoparticle agglomerates. Researchers have used various empirical equations to determine various properties of the particles being fluidized. Among them are the Ergun equation and its variations which are used to predict the minimum fluidization velocity (u_{mf}) and the bed pressure drop. Another widely used empirical equation is based on the work of Richardson and Zaki (1954) which showed that when the volumetric flux is plotted as a function of the terminal velocity and bed voidage on a logarithmic scale, it yields a linear relationship.

One of the dominant works on the conventional fluidization of nanoparticle agglomerates was done by Yao et al (2002). They investigated six SiO2 powders with primary particle sizes of 7-16 nm, and found that the conventional fluidization of the nanoparticle agglomerates were not Geldart Class-C (Cohesive) behavior like, but rather displayed smooth fluidization and high bed expansions which obeyed the Richardson-Zaki equation. They also found low values for the minimum fluidization velocity in the order of 1 cm/s to 10 cm/s, but even at these low velocities, elutriation of the agglomerates was observed. They also observed that the nanoparticles link into a tri-dimensional netlike structure which coalesces into simple agglomerates of micron size and the simple agglomerates then form larger complex agglomerates.

Despite the high bed expansions and low u_{mf} values obtained by Yao et al (2002), elutriation of bed particles was still a significant problem. Subsequent research showed

that by coupling conventional fluidization with an external field, these results could be improved. Zhu et al. (2004) investigated the effect of sound on the fluidization behavior of fumed silica nanoparticles (Degussa Aerosil© R974, having a primary particle size of 12 nm) in the form of large 100–400 micron agglomerates. They found that by the application of sound wave excitations at low frequencies, the bed of nanoparticle agglomerates can be readily fluidized and the minimum fluidization velocity was significantly reduced. For example, the minimum fluidization velocity decreased from 0.14 cm/s in the absence of sound to 0.054 cm/s with the assistance of sound. In addition, under the influence of the sound, channeling disappears and the bed fluidized more uniformly. However, at frequencies above 2000 Hz, the propagated sound wave had no impact on the fluidization behavior.

Nam et al. (2004) achieved homogeneous fluidization of agglomerates of nanoparticles by coupling aeration with vibration. Their experimental data, showed a reduction of the minimum fluidization velocity, an increase in bed height, and a decrease in elutriation and bubbling. They also observed an increase in the stabilization of the fluidized bed which was shown by the extension of the settling time after the vibration was shut down. The Richardson and Zaki (R-Z) equation was applied to the fluidization of nanoparticle agglomerates by Nam et al. (2004). In their application, they used a fractal analysis to estimate the number of primary particles within the agglomerates and by selecting the proper R-Z exponential index, estimated the agglomerate size.

More recently Zhu et al. (2005) performed an experimental study to determine the effect of eleven different types of nanoparticles on the gas fluidization characteristics of their respective agglomerates. They used an optical technique to visualize the behavior,

as well as to measure the sizes of the fluidized nanoparticle agglomerates present at the bed surface. They reported that APF type agglomerates could expand as much as five times the initial bed height as the superficial gas velocity was increased, thus corroborating the observation made by Yao et al. (2002) and Nam et al. (2004). In addition, they found that ABF agglomerates fluidize with large bubbles present and show very little bed expansion. They developed a model to predict the agglomerate sizes for APF nanoparticles, and the results agreed fairly well with the optical measurements.

Hakim et al. (2005) also performed studies on the fluidization behavior of agglomerates of nanopowders with a vibration setup. They found that mechanical vibration can be used to reduce the size of the agglomerates, improve the quality of fluidization, and in contrast to changing the pressure at which the experiment was conducted, it has a larger effect on the minimum fluidization velocity which agreed with the observation made by Nam et al. (2004).

Yu et al. (2005) observed the fluidization behavior of agglomerates of nanoparticles in a mixture with magnetic particles under the influence of an oscillating magnetic field. The magnetic particles resided at the bottom of the bed, and served mainly as a means to break down the larger agglomerates. Previous work done using this method involved fluidizable magnetic particles. With the magnetic assistance, the bed of nanoparticle agglomerates was smoothly fluidized and the minimum fluidization velocity was appreciatively reduced. In addition, it was noted that channeling or slugging of the bed disappeared and the bed expanded uniformly without bubbles, and with negligible elutriation.

Guo et al. (2006) also reported improvement to the fluidization of these nanoparticle agglomerates by the influence of an acoustic field. In their work, they used 5-10 nm SiO2 Nanoparticles with and without surface modification by an organic compound. They found that in a packed bed the sound wave energy had significant effect on the compaction of the bed. They also found that in a bed of nanoparticle agglomerates, the minimum fluidization velocity was reduced significantly with increasing sound frequency, and then later rose with the frequency, and that the acoustic field had a better effect on the particles with surface modification.

In a rotating fluidized bed assembly, enhanced fluidization of nanoparticle agglomerates was also observed by Quevedo et al. (2006). Their experiments were carried out at different rotating speeds corresponding 10, 20, 30 and 40 times the gravity force (9.8 m/s^2). It was found that the fumed silica agglomerates expanded considerably while the TiO$_2$ agglomerates showed very little bed expansion. The minimum fluidization velocities for Aerosil R974 and R972 ranged from 0.02 to 0.07 m/s and from 0.13 to 0.20 m/s for Aeroxide TiO$_2$, but at high rotating speeds, the minimum fluidization velocity increased for all the powders

Levy et al. (2006) combined the effect of both mechanical and high intensity acoustic vibrations to fluidize fine cohesive powders of which included 12 nm Aerosil. They also found a decrease in the superficial gas velocities needed to achieve minimum fluidization, and by comparison found the acoustic vibrations to be more effective than horizontal mechanical vibrations.

Lastly, Wang et al. (2006) focused on determining the size of the fluidized aggregates and the effect of superficial gas velocity on particle aggregation in a fluidized

bed of nanoparticles. In their experiments, they fluidized Degussa Aerosil R974 powder, with a primary particle size of 12 nm in a glass column. Their in situ images, obtained with a high-resolution digital CCD camera, showed that the nano-agglomerates had a wide size distribution and contained a significant component of very small sized particles. The mean size of the aggregates was found to decrease with increasing superficial gas velocity, while the mean sphericity of the aggregates was found to be insensitive to changes in the superficial gas velocity.

This present research continues the work on assisting methods to enhance the fluidization of nanoparticle agglomerates. It introduces a new method for improving the quality of fluidization of nanoparticle agglomerates by the use of downward pointing jets.

1.4 Concepts in Conventional Fluidization

As mentioned earlier, the fluidization phenomenon is the suspension of a bed of solid particles by a fluid, and in the fluidized state, the bed acquires fluid-like properties. The onset of fluidization is generally referred to as minimum fluidization. One very popular demonstration of this phenomenon is that of a plastic duck immersed in a bed of sand particles (Gibilaro, 2001). Air from a source is progressively sent through the bed in order to get it dispersed. When the bed becomes fluidized, the duck could be seen floating on the bed as it would, if it were immersed in water. A pictorial view found in several publications describing the behavior of different beds is shown in Figure 1.1. The figure basically explains what happens to a bed of fluidizable fine particles as the upward flow of gas is progressively increased until the gas velocity exceeds the terminal velocity of the particles and bed is conveyed out of the column.
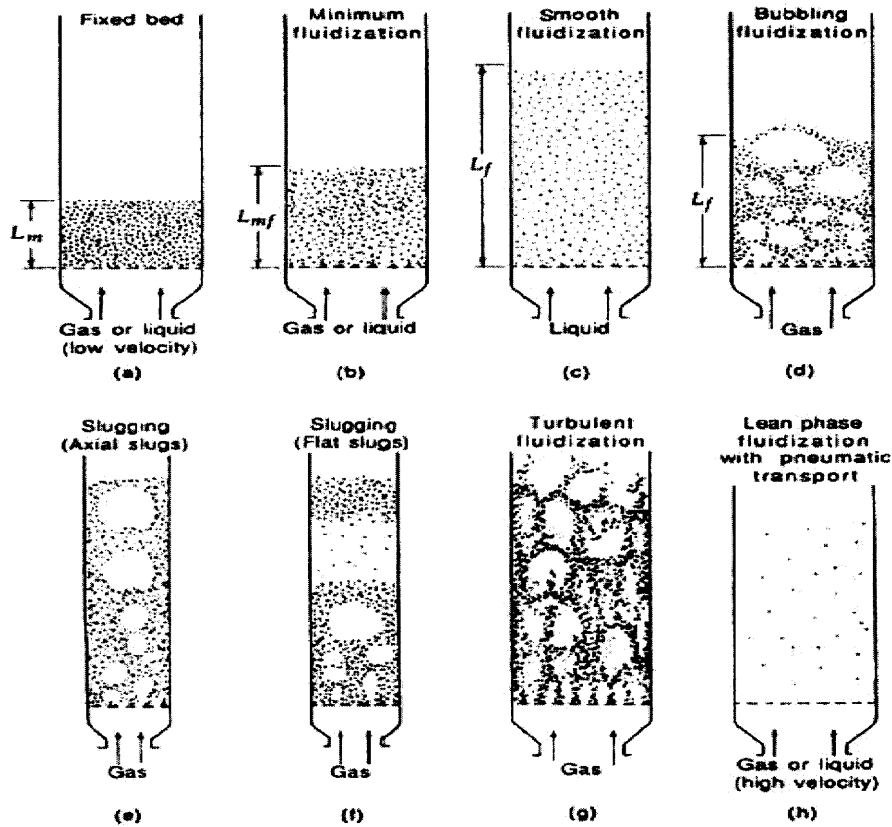
Figure 1.1 Various Gas-Solid contacting patterns (Kunii et al. 1991).

Figure 1.1(a) shows that the upward flowing gas does not possess enough drag force to suspend the bed of particles so the bed behaves as a packed bed. At some point while the velocity of the gas is still being increased, the pressure drop across the bed will equal the weight of the bed of particles. This point is called the minimum fluidization velocity (u_{mf}) and is illustrated by Figure 1.1(b), and the fluidization is usually homogenous and smooth. While the flow of fluid is still been increased, the bed responds by gaining in bed height Figure 1.1(c). Further increase of the upward flow of the gas, leads to formation of bubbles which tend to coalesce as they move up the bed. The velocity at which bubble formation is observed is called the minimum bubbling velocity (umb).

It has been observed that some particles do not show the smooth and homogenous type fluidization observed in Figure1.1b and c, (Zhu et al. 2005). In deep beds with small diameter, coalescence of bubbles may lead to slugging Figure 1.1(e − g). At very high flow rates, the terminal velocity of the particles is exceeded, intense agitation develops and the surface of the bed is observed as a blur. This, as shown in Figure 1.1g is called turbulent fluidization, and a further increase in the velocity leads to a dilute phase with pneumatic transport of solids (Kunii et al., 1991).

The illustrations shown in Figure 1.1, each represents a different fluidization environment and contacting between the phases involved. The difference of the response of each environment to increasing fluid flow is a representation of the term commonly known as fluidization quality. Also factored into the term, is the ease with which particles fluidize, the range of conditions necessary to keep the particles fluidized, and other factors which affect fluidization in general.

1.4.1 Classification of Particles

It has already been stated that fluidization behavior reflects the nature of the particle and fluid in contact with each other. Hence, different particles tend to behave very differently while being fluidized. For gas phase fluidization, a well known classification was done by Geldart (1973). Particles were classified into groups based on their fluidization behavior. The characteristics of the particles established boundaries which defined 4 different groups. This classification is shown Figure 1.2.
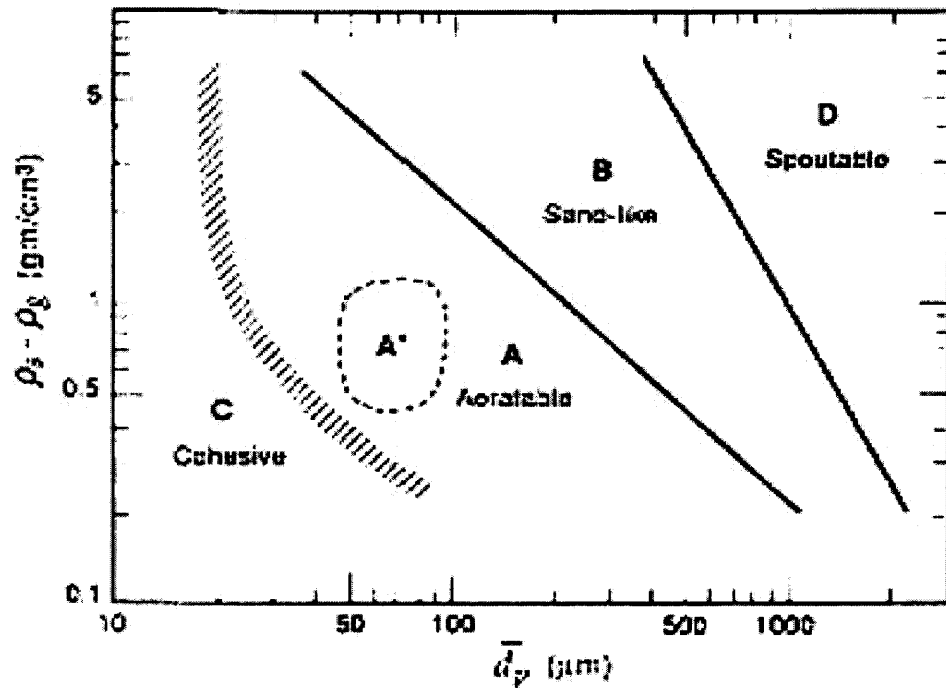
Figure 1.2 Classification of particles by Geldart.

According to Geldart, group A particles can be smoothly fluidized at velocities greater than the minimum fluidization velocity without bubbles. Gas bubbles begin to appear at the minimum bubbling velocity, while for group B particles gas bubbles tend to appear immediately at the minimum fluidization velocity. The group C particles, also known as the cohesive particles, are very difficult to fluidize, and group D particles easily form stable spouted beds.

Some of the boundaries separating the various groups can be represented by mathematical expressions (Geldart, 1973). For example, the particles are in group A if

$$\frac{8\times10^{-4}gd_p(\rho_p - \rho_f)}{K\mu} \leq 1 \qquad (1.2)$$

Equation (1.2) represents the boundary between group A and group B particles, and the particles are in group D if

$$\frac{8\times10^{-4}(\rho_p - \rho_f)gd_p^2}{\mu\varepsilon_{mf}} \geq U_B \tag{1.3}$$

Equation (1.3) represents the boundary between group B and group D particles. Another important classification taking inter-particle cohesive forces into account was done by Molerus (1982). The equations separating the different boundaries are given below.

$$10\times\frac{(\rho_p - \rho_f)d_p^3 g}{F_H} = K_1 \qquad \text{Boundary for group A and C} \tag{1.4}$$

$$\frac{\pi(\rho_p - \rho_f)d_p^3 g}{6F_H} = K_2 \qquad \text{Boundary for group A and B} \tag{1.5}$$

$$\frac{(\rho_p - \rho_f)d_p g}{\rho_f U_{mf}^2} = K_3 \qquad \text{Boundary for group B and D} \tag{1.6}$$

In each of the equations, the constants K depends on the type of powder and other factors while F_H is a representation of the inter particle cohesive force.
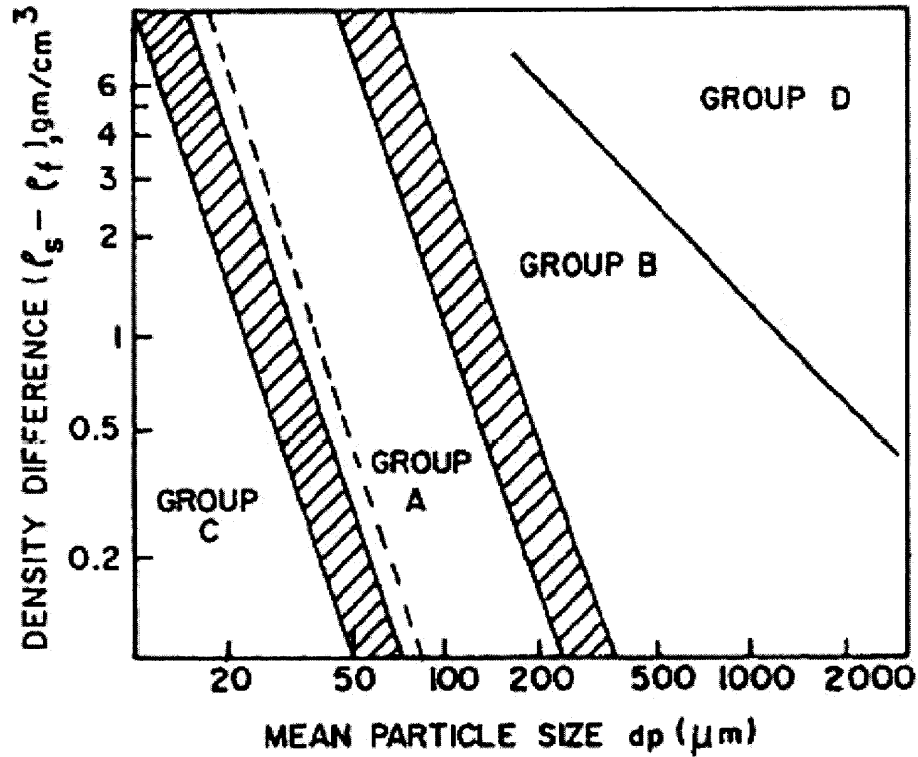
Figure 1.3 Modified classification of the Geldart boundaries between different classes of powders by Molerus. (1982)

The hatched areas between group A and C and group A and B represent different hardness of the particles. The dotted line between group A and C represents the effect of aggravations which consolidate the powder, and shifts the AC boundary.

According to the additional data analyzed by Grace in 1986, new boundaries between groups A and B, and groups B and D were suggested.

$$Ar = 1.03 \times 10^6 (\frac{\rho_p - \rho_f}{\rho_f})^{-1.275}$$ Boundary for group A and group B   (1.7)

and

$$Ar = 1.45 \times 10^5$$ Boundary for group B and group D   (1.8)

where Ar is the Archimedes number

Goossen (1998) classified the boundaries on the basis of the Archimedes number. The boundaries are

Group C boundary	$Ar = 0.97$	(1.9)
Group A/C boundary	$Ar = 9.8$	(1.10)
Group A/B boundary	$Ar = 88.5$	(1.11)
Group B/D boundary	$Ar = 176,900$	(1.12)

These four suggested boundaries compare well with Geldart's and Molerus' boundaries especially when the fluid involved is air.

1.4.2 Pressure Drop and Minimum Fluidization Velocity, (u_{mf})

The pressure drop across the bed is a representation of the driving force for fluidization. It also signifies how much work the fluid is doing, and it is expected that as the superficial gas velocity increases, so does the pressure drop. However upon reaching the fluidized state, the particles are entirely supported by the fluid and the pressure drop is equal to the weight of the bed divided by the cross sectional area of the fluidization column. This event is better described graphically as in Figure 1.4.
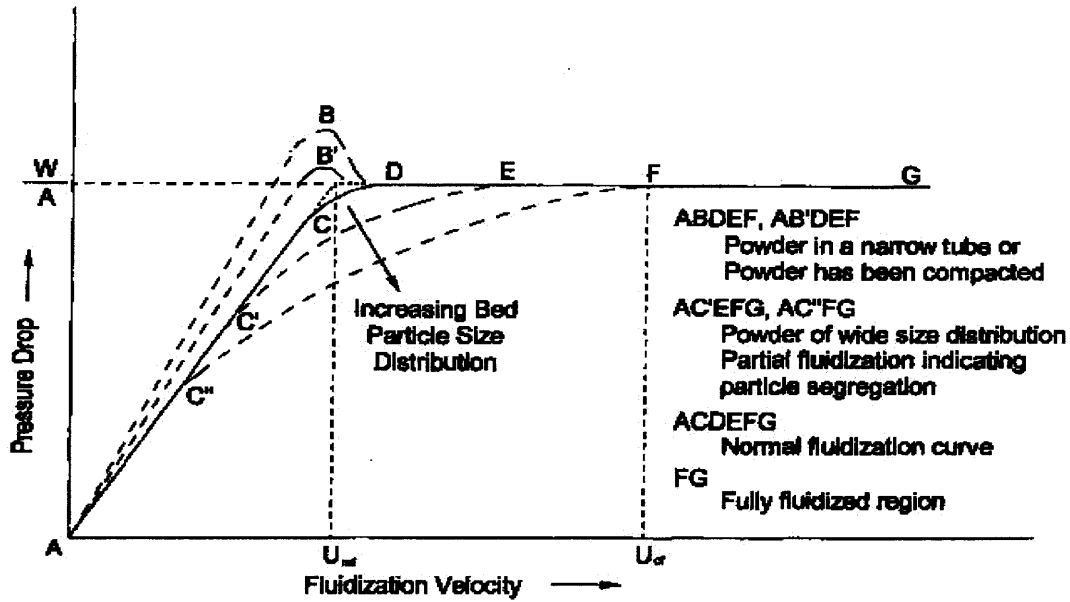
Figure 1.4 Typical observations for pressure drop vs. gas velocity plot (Yang, 2003).

Normally, the fluidization behavior would be represented by the curve ACDEFG. The prefluidization regime, where the pressure drop increases linearly with the gas velocity is represented by the boundary ACU_{mf} in the figure. In this domain, the bed typically behaves like a packed bed, and the pressure drop can be represented by the Ergun equation

$$g_c \frac{\Delta P}{L_m} = 2\rho_f \frac{u_0^2 [f_{pL} + f_{pT}]}{\phi_s d_p}$$

(1.13)

where the friction factor contribution for laminar flow is

$$f_{pL} = \frac{75}{\text{Re}_p} \left[\frac{(1-\varepsilon)}{\varepsilon^3} \right]$$

(1.14)

and the friction factor contribution for turbulent flow is given by

$$f_{pT} = 0.875 \left[\frac{(1-\varepsilon)}{\varepsilon^3} \right] \qquad (1.15)$$

with

$$\text{Re}_p = \frac{\rho_f \phi_s d_p u_0}{(1-\varepsilon)\mu} \qquad (1.16)$$

Upon reaching the fluidized state the weight of the bed is suspended by the drag exerted by the fluid. At this point, the weight of the bed is equal to the cross sectional area of the fluidized bed multiplied by the pressure drop, and with further increase in the superficial gas velocity, the pressure drop stays relatively constant. The pressure drop in the fluidized state is given by

$$g_c \frac{\Delta P}{L_{mf}} = (1 - \varepsilon_{mf})(\rho_s - \rho_f)g \qquad (1.17)$$

In the case of nanoparticle agglomerates, the flow through the bed prior to fluidization could be highly irregular and the Ergun equation becomes inapplicable. These agglomerates exhibit channeling and tend to lift as a plug which tampers with the pressure drop readings. However, once the drag of the fluid is enough to suspend the particles, the pressure drop becomes relatively constant.

This pressure drop is very important because it is an indication of the state of the fluidized bed. In a scenario where the expected pressure drop does not match the weight of the bed, it could be due to gas bypass in the form of bubbles, entrainment of particles from the bed, leaks, and system malfunction. Powder sticking to the wall of the column and not participating in the fluidization due to electrostatic charge build up, non uniform flow of fluid through the distributor, and formation of a layer of particles (cake) above the distributor may also contribute to a lowering of the pressure drop.

The minimum fluidization velocity, u_{mf} is the velocity corresponding to the onset of the homogenous suspension of a bed of particles. However, in some cases, the bed appears to simply bubble. At this velocity, the void fraction of the bed increases, the pressure drop across the bed approximately equals the weight of the bed particles, and fluidized bed expands and acquires liquid like behavior. The u_{mf} can be seen in Figure 1.4 as the inflection point of the curve ACDEFG. The theoretical determination of the minimum fluidization velocity is achieved by combining equations 1.13 and 1.17 which yields

$$Ar = \frac{150(1-\varepsilon_{mf})}{\varepsilon_{mf}^3 \Phi_s^2} Re_{p,mf} + \frac{1.75}{\varepsilon_{mf}^3} Re_{p,mf}^2 \tag{1.18}$$

with dimensionless variables

$$Re_{p,mf} = \frac{d_p u_{mf} \rho_g}{\mu} \tag{1.19}$$

and

$$Ar = \frac{d_p^3 \rho_g (\rho_s - \rho_g) g}{\mu^2} \tag{1.20}$$

It has been found that for particles with $Re_{p,mf} < 20$, equation (1.18) can be simplified into

$$u_{mf} = \frac{d_p^2 (\rho_s - \rho_g) g}{150\mu} \frac{\varepsilon_{mf}^3 \Phi_s^2}{1 - \varepsilon_{mf}} \tag{1.21}$$

With respect to the Reynolds number (Re) and the Archimedes number (Ar), equation (1.18) can be further reduced to

$$\text{Re}_{p,mf} = \sqrt{C_1^2 + C_2 Ar} - C_1 \tag{1.22}$$

where the constants C_1 and C_2 can be found in the literature. Some typical values suggested by different researchers are tabulated below.

Table 1.1 Values for constants C_1 and C_2 (Yang, 2003)

Reference	C_1	C_2
Wen and Yu (1966)	33.7	0.0408
Richardson (1971)	25.7	0.0365
Sexena and Vogel (1978)	25.3	0.0571
Babu et al. (1978)	25.25	0.0651
Grace (1982)	27.2	0.0408
Chitester et al. (1984)	28.7	0.0494

Other existing simplifications state that: For $Ar < 10^3$

$$\text{Re}_{p,mf} = 7.5 \times 10^{-4} \, Ar \tag{1.23}$$

And for $Ar > 10^7$

$$\text{Re}_{p,mf} = 0.202 \, Ar^{0.5} \tag{1.24}$$

For an actual fluidization operation, the measured pressure drop across the fluidized bed at the minimum fluidization point usually differs from the norm. This behavior is also represented in Figure 1.4. For example, for a bed made up of a wide distribution of particles, the appropriate curve would be AC'EFG.

For most particles, when the bed becomes fully fluidized, the pressure drop should be relatively constant. (Curve FG in Figure 1.4). In cases where elutriation of bed

particles is present, the actual pressure drop would start to slope downwards after significant entrainment of particles from the surface of the bed occurs. Figure 1.5 shows the response of the pressure drop and bed height for different classes of powders with regards to increasing gas flow.
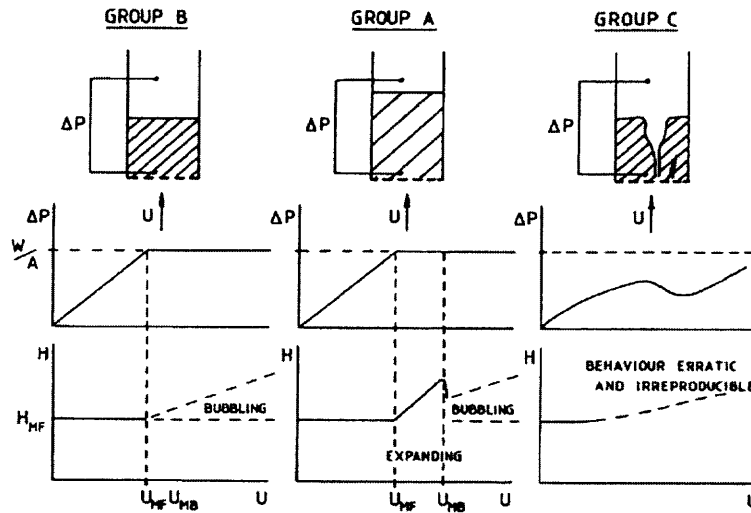
Figure 1.5 Fluidization of different classes of powders (Kunii et al. 1991).

It should be noted that some of the variables used in the calculation of the minimum fluidization velocity are pressure and temperature sensitive. Hence, it follows that both pressure and temperature affect the fluidization behavior of a bed of particles. For example, by increasing the operating pressure of system, researchers found that the u_{mf} decreases and the bed voidage increases. This was found to be true particularly for particles of size 360 μm (Kunii et al. 1991)

1.4.3 Settling Velocity

The settling velocity for a single particle suspended in a fluid represents the velocity at which the force balancing the weight of the particle reaches a critical value, at which any further increase of the flow results in the acceleration of the particle. When a particle falls

through a fluid, its settling velocity reaches a critical point, where there is no acceleration. This critical velocity is known as the terminal velocity. In a fluidized bed of particles, this critical point represents the velocity at which the carryover of particles is observed. The equation for the terminal velocity is derived from a force balance on the particle.

The terminal velocity is given by

$$u_t = \left[\frac{4 d_p (\rho_s - \rho_g) g}{3 \rho_g C_D} \right]^{1/2}$$

(1.25)

where the drag coefficient can be found from

$$C_D = \frac{24}{Re_p} + 3.3643 Re_p^{0.3471} + \frac{0.4607 Re_p}{Re_p + 2682.5}$$

(1.26)

There are many established equations for estimating the value of the drag coefficient and the terminal velocity for different particulates. Their differences are based on particle porosity, regularity, density, etc. A simplification of equation (1.25) for irregular particles (Kunii and Levenspiel, 1991) gives

$$U_t^* = \left[\frac{18}{(d_p^*)^2} + \frac{2.335 - 1.744 \Phi}{(d_p^*)^{0.5}} \right]^{-1} \qquad \text{where} \quad 0.5 < \Phi < 1$$

(1.27)

and for spherical particles reduces to

$$U_t^* = \left[\frac{18}{(d_p^*)^2} + \frac{0.591}{(d_p^*)^{0.5}} \right]^{-1} \qquad \text{where} \quad \Phi = 1$$

(1.28)

In most experiments, the critical point for the terminal velocity is usually observed by the blurring of the interface between the fluidized particles and the fluid space.

1.4.4 Bed Expansion (L_B) and Voidage (ϵ)

As the flow of fluid within the bed is progressively increased, bubbles generated within the bed fill up and occupy space. This usually leads to an increase in the voidage of the bed and consequently, the expansion of the bed. The observed bed expansion is usually dependent on the nature and class of the powder involved.(Yang, 2003)

Prior to reaching the minimum fluidization point, minimal bed expansion is observed, and the bed voidage is constant. The bed voidage ϵ is dependent on parameters such as the particles size, shape, distribution, and coarseness. Normally, smaller particles have lower terminal and settling velocities. These cause bed voidage to increase, however by shaking, or tapping they can be compacted (Gupta, 1999).

Based on reported observations, it has been widely shown that the plot of U which is the volumetric flux against the bed voidage on a logarithmic scale, yields points on a straight line. A description of this observation could be stated as

$$U = U_i \varepsilon^n \tag{1.29}$$

This equation is based on the extensive work of Richardson and Zaki, and is universally known as the Richardson-Zaki equation (Gibilaro, 2001). This empirical equation has been modified to fit the purpose of nanoparticle agglomerate fluidization based on the fractal structure analysis (Nam et al. 2004)

This chapter introduced the various hydrodynamic principles and references related to the conventional fluidization of both micron sized and nanoparticles. For most of the experiments, the jet assisted fluidization is compared to the conventional fluidization mode. The primary difference between the two modes is the presence of a secondary gas line equipped with a nozzle which is inserted into the bed. The principles covered will also be useful in evaluating the performance of the jet assisted mode. The next chapter will present concepts which are pertaining to jets. This includes a discussion on the jet penetration depth, jet coalescence and other principles, which are necessary for a better understanding of the behavior of jets in fluidized beds.

CHAPTER 2

INTRODUCTION: CONCEPTS IN JET ASSISTED FLUIDIZATION AND THE USE OF INTERNALS

2.1 Overview

The use of jets in fluidized bed has been studied for quite some time. Most notable is the jetting fluidized bed, where the jet is generated at the gas entry region of the fluidized bed. In applications prior to this work, the jets were generated from orifices larger than 500 microns, and at velocities lower than 100 m/s. Jets usually emanate from nozzles within the bed, and are generally employed in fluidization to facilitate mixing, contacting of the solid and gas phases, improvement of heat and mass transfer, and to break-down particles into smaller sizes.

The effect of these nozzles, their orientation, and configurations, within the bed is the focus of various studies, primarily because the hydrodynamic response of the fluidized bed is largely affected by the flow from the jet. The configurations found in the literature are horizontal insertion, vertical upward, vertical downward towards the distributor and the insertion of the nozzle at an inclined angle upwards or downwards. In this work, we considered different configuration of nozzles for generating the jet, and from our results it was possible to develop an optimal configuration for specific nanopowders. This form of jetting phenomena is known as a gas-solid two phase jet (Yang, 2003). Performance, in this regard is usually determined by the entrainment rate of both the gas and the solid, and the characteristic jet penetration region. However, there is some disparity regarding what exactly constitutes a jet within a fluidized bed. In some experiments jets are seen to penetrate the bed of particles in the form of oscillating

bubbles, called a pulsating jet, while in others, permanent flame-like jets are observed. The type of jet formed is said to depend on the properties of the gas, the powder and the operation conditions.

Also widely applied in fluidized bed technology, is the use of internals such as baffles and highly efficient internal tubes. These are used to improve the performance of fluidized beds by affecting the gas solid contacting pattern. In this work we also coupled the use of internals with conventional and jet assisted aeration to improve the performance of the gas fluidization of nanoparticle agglomerates.

2.2 Literature Review regarding the Use of Jets in Fluidized Beds

Many researchers over the years have contributed to the study of the behavior and use of jets in gas fluidized beds. Most of their work focuses on the determination of the jet penetration depth, momentum dissipation, angle or half angle, velocity profiles, bubble size, and bubble frequency. Rowe et al. (1970) performed experiments with different powders in a fluidized bed with a secondary injection nozzle which could be oriented in the downward or upward position. They used nozzles with sizes ranging from 6.4 to 15.9 mm, and operated at jet velocities as high as 70 m/s. They observed that gas was issued from the nozzle's single orifice in the form of bubbles.

Behie et al. (1970) studied the jet momentum dissipation at a grid of a large fluidized bed with nozzles varying from 0.25 inch to1.25 inch in internal diameter. They found a relationship between the axial momentum of the jet and a modified Froude number. Later, Blake et al. (1990) proposed a model for relating various hydrodynamic parameters to the jet penetration height for spherical particles in a non-compressible

medium. The model included physical variables such as gas density, solid density, jet velocity, particle diameter, bed dimension, gravity and gas viscosity.

Shen et al. (1990) experimented with a single downward nozzle inserted into a fluidized bed of sand particles. It was observed that the air discharging from the nozzle formed a stable core which extended downward by about 5 cm. It then reversed direction and flowed upwards along one of the external walls of the nozzle, and thus forming a side jet which was established at the nozzle wall. A smaller fraction exited at the other side forming bubbles which rose through the bed, and a few seconds later, the jet switched sides again.

Xuereb et al. (1991) observed the behavior of downward facing, upward facing and horizontal configurations of the nozzle. They studied the effect of the fluidization velocity, gas injection velocity and particle diameter for each configuration, and they confirmed that there was a dragging zone of particles from the dense phase into the jet.

In another application, Werther et al. (1993) studied the mechanism of jet attrition in a gas fluidized bed for two different particles. It was found that the attrition rate depended on whether the jet is issued into a pre-fluidized bed or into a non-aerated bed.

Hong et al. (1995) developed a two phase model describing gas-solid flow macroscopically in a fluidized bed. They found that the jet penetration height increased with increasing jet velocity, but at much higher velocities the corresponding response of jet penetration height was slower.

Cleaver et al. (1995), conducted experiments using X-ray imaging techniques to measure the angle for a vertical jet as it entered a fluidized bed. They found that the jet angle decreased with increasing operating pressure, decreasing bed temperature, and also

with increasing orifice gas velocity. The dependence of orifice size on the jet angle was ambiguous, although larger orifice sizes resulted in significantly larger jet angles in some cases.

For a different application Choi et al. (1996) found in their experiment that gas issued from a 25mm secondary horizontal nozzle reduced the rate of entrainment of particles in their fluidized bed.

Hong et al. (1996) experimented with a vertical jet in the center and an inclined jet at the side of a fluidized bed. They examined the influences of jet velocity, nozzle diameter, inclination angle and position of the nozzle on the jet penetration length. They also obtained a correlation for the inclined jet penetration based on experimental data. Chyang et al. (1996) investigated the jetting discharge modes formed at a single horizontal nozzle inserted into the fluidized bed. They found that the jet penetration length increased with the gas velocity through the nozzle, and the nozzle diameter.

Vaccaro (1997a) did a dimensional analysis of the operating variables and equations found in the literature related to the formation of a jet above an upward gas discharging nozzle in a fluidized bed. The dimensional analysis yielded a set of relevant dimensionless groups, among which includes, the two-phase Froude number which provides a good correlation of most of the literature data. This was also found experimentally by Yang (1998). Vaccaro et al. (1997b) also developed an approach for determining the jet penetration length based on the statistical analysis of pressure signals taken simultaneously on the jet axis and at the side wall of the bed.

Yang (1998) studied the momentum dissipation, jet penetration depth, and jet velocity profiles in a 30-cm and a 3-m diameter semicircular fluidized bed. The gas

interchange between the jet and the emulsion phase of the fluidized bed was investigated by the injection of helium or carbon dioxide as a gas tracer. The two-phase Froude number was found to be applicable for large jets up to 255-mm to correlate the jet penetration depth.

Tasirin et al. (1999) studied the effects of free jet velocity, separation distance and the geometry of the set-up on the initial rate of grinding of coarse cracking catalyst particles using 2 mm id nozzles.

Guo et al. (2001a) studied the flow behavior of the jet regime, the effects of particulate density, particulate diameter, jet velocity, static bed height, nozzle diameter (8-16 mm), and annular gas flow rate on the flow regime transitions. They found that the jet penetration depth decreased when the annular flow rate was in the range of 1-2.5 times the minimum fluidization velocity, and remained constant for flow rates between 2.5-3.0 times the minimum fluidization velocity. Another study (Guo et al, 2001b) was done with two upward facing vertical nozzles. In conducting their research they utilized a frame by frame analysis of experimental videos. The observed flow patterns were separated jet, flow transition, and jet coalescence which all depended on the distance between the nozzles and jet gas velocity. Later work by Guo et al. (2002) made use of pressure signals to investigate flow transition. Their result shows that the jet flow transition velocity corresponds to the peaks in their frequency vs. jet velocity plot.

Hong et al. (2003) also studied the formation and coalescence of jets in a gas-solid fluidized bed with two vertical jets. In their experiments they found that the jet penetration height increased with the increase of the superficial gas velocity, and they were able to obtain correlations for estimating the penetration height of the jet. More

recently, Hong et al. (2005) presented both experimental and numerical studies on the hydrodynamic behavior of fine powders in jet fluidized beds with different configurations of jets. They concluded that a single downward jet located inside the bed gave better mixing of the particles and broke up the agglomerates.

In their investigation of the jet penetration depth, Zhong et al. (2005) used a two-dimensional cold model of a spout–fluidized bed with a cross section of 300 mm×30 mm and height of 2000 mm. They used four types of Geldart group D particles as bed material, and a multi-channel pressure sampling system and a high-resolution digital CCD camera were employed for experimental investigations. The effects of gas velocity, nozzle diameter, static bed height, particle property and fluidizing gas flow rate on the jet penetration depth were systematically studied by pressure signal analysis and image processing. Their results indicated that the jet penetration depth increased with increasing gas velocity and nozzle diameter, but it decreased with increasing particle density, particle diameter, static bed height and fluidizing gas flow rate. Additionally, they proposed a new correlation for predicting the jet penetration depth in spout–fluid beds which considered all of the listed effects especially static bed height and fluidizing gas flow. The correlation was compared with published experimental data and correlations, and was found to be in good agreement.

Tadashi et al. (2006) studied the characteristic grinding mechanism of Ethenzamide particles. The grinding rate was found to be affected by operating parameters such as the grinding gas pressure, the weight of raw material and the linear velocity at the grinding nozzle.

In this work, different configurations of micro nozzles with orifice sizes in the range of 127 to 508 μm were used to improve the fluidization behavior of nanoparticle agglomerates. Best results were obtained in configurations where the nozzle pointed downwards, and was relatively close to the distributor. Under the influence of the jet, the minimum bubbling velocity was delayed, bed expansion increased a lot, fluidization quality improved, and better dispersion was observed.

2.3 Concepts and Terms related to Jets and Internals

As mentioned earlier jets are used in fluidized beds to facilitate mixing, contacting of solid and gas phases, to improve heat and mass transfer and to break-down particles into smaller sizes. They usually emanate from nozzles which are installed within the bed, and their many configurations have received wide research attention. In order to fully understand the behavior of the jet, properties such as the jet profiles, jet penetration depth, jet angle, bubble size and frequency, and the jet separation distance, transition and coalescence velocities will be defined. In this work, the use of internals was also studied. Internals such as baffles, highly efficient internal tubes, packing, and insert bodies are used in fluidization to improve the uniformity of flow, enhance gas solid contacting and mixing, and reduce carryover of particles (Yang, 2003).

2.3.1 Jet Momentum Dissipation

The process by which jet flows lose their initial momentum and transfer mass and energy to their surrounding environment is called jet momentum dissipation, and this interaction occurs along the entire length of the jet to various extents (De Young, 2004). It is present

when ever the jet is moving relative to the surrounding bed of particles. This interaction influences the transfer of mass, momentum and energy between the jet and the environment, and an understanding of its details is a reliable way to determine and quantify the jet behavior (De Young., 2004, Vaccaro,1997).
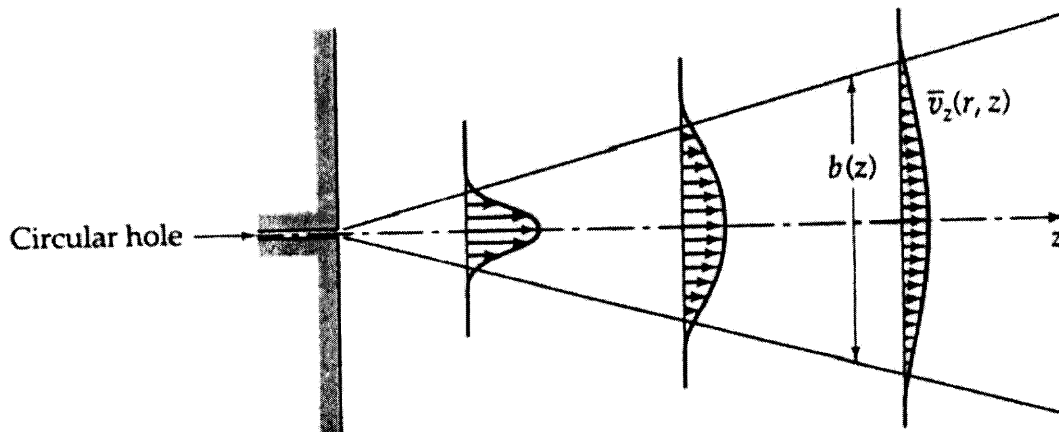
Figure 2.1 Circular jet emerging from a plane wall. (Bird et al., 2002).

Theoretically, it is expected that as a jet emerges from a circular nozzle or wall as in Figure 2.1, the velocity profile would be similar in shape along the z -axis, and each profile would be related by a scaling factor. It is also expected that the velocity should be maximum at the centerline, and it should decrease radially away from the centerline. Figure 2.2 shows a picture of a fully developed turbulent jet

Figure 2.2 Example of a fully turbulent Jet (De Young, 2004).

In the application of jets to the fluidized bed, it has been observed by some researchers that at some point along the axial direction, the turbulent jet degenerates into bubbles which eventually lose their momentum (Behie et al, 1970). According to Yang., (1998), the dissipation of the centerline velocity in a fluidized bed can be calculated from the following equation:

$$\frac{U_j}{U_m} = 0.26 \frac{x}{d_o} \tag{2.1}$$

where Um is the maximum jet velocity at the axis

The equation shows an inverse relationship between the maximum jet velocity and the axial distance which implies a decay of momentum in the axial direction as the jet penetrates the bed This relationship is also evident in Figure 2.1 which shows a shortening of the maximum jet velocity with increasing values of z.

2.3.2 Jet Penetration Depth

In some experiments, jets have been observed in the form of elongated, oscillating bubbles, called a pulsating jet (Rowe et al., 1979, Yang., 2003) while in other cases permanent flame like jets were observed (Rowe et al., 1979). Experimentally, the determination of the jet penetration length has been done using techniques which include, the pressure signal analysis, and the use of radiation densimeters (Vaccaro et al, 1997b). In the pressure signal analysis method, pressure fluctuations induced by gas discharge through an upward nozzle in a fluidized bed are analyzed, and in one use of radiation desimeters, X-rays are passed through the bed, and the resulting image is photographed with a high speed cine camera.

Knowledge of the jet penetration length in fluidized beds is relevant to determine the minimum distance from the nozzle at which bed internals, such as tube banks and baffles, can be safely located to prevent erosion by the gas-solid mixture (Vacacro et al, 1997).
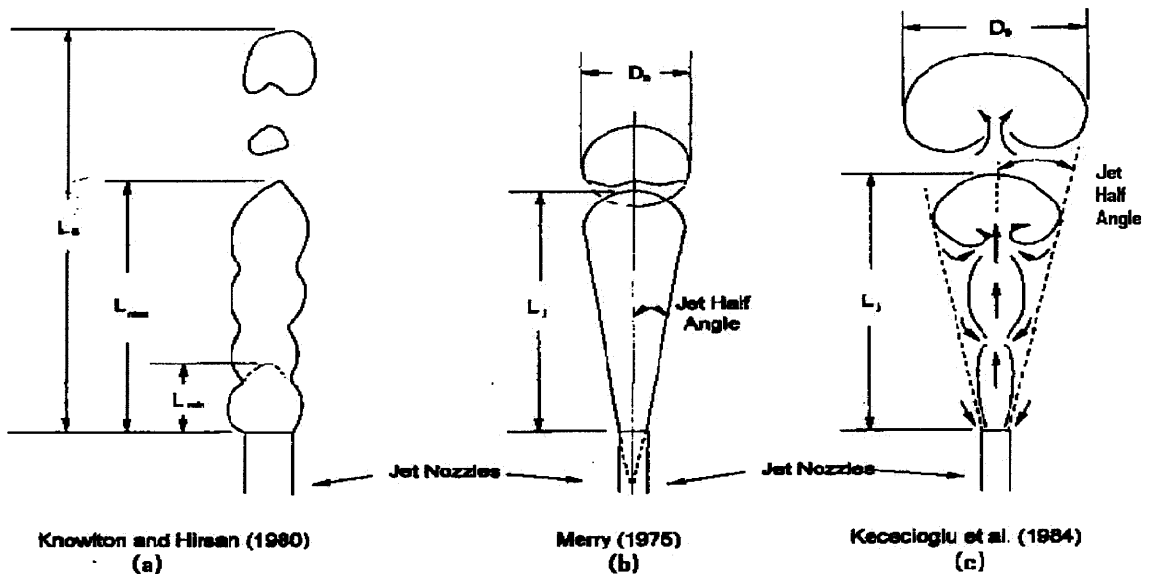
Figure 2.3 Different jet penetration depths (Yang, 1998).

Figure 2.3 shows the difference between the kinds of jet penetration that has been reported in literature. Lmax is the penetration depth of a series of interpenetration cavities, L_B is the deepest penetration depth of jet bubbles, and Lmin is the shortest jet penetration height observed (Zhong et al, 2005). The type of Lj measured is also dependent on the measuring technique. Visual inspection usually yields Lmax. Techniques making use of probes, also measure Lmax, and as such are consistent with measurements done by visual techniques. The measurements done with the aid of pitot tubes has lead to considerable debate, because although its determination is based on the indirect measurement of gas momentum, some results have suggested similarities to Lmax. However, with pressure signal analysis, the L_B value is obtained (Zhong et al 2005).

According to Yang and Keairns (1978), the jet penetration depth could be correlated to the two-phase Froude number, although at the time, the equation lacked a theoretical basis. The equation proposed was

$$\frac{L_j}{d_o} = (Fr)^{0.5} \qquad (2.3)$$

Where

$$(Fr) = \left[\frac{\rho_f}{\rho_p - \rho_f} \frac{U_j^2}{g d_o} \right] \qquad (2.4)$$

Presently, there are many correlations found in the literature for evaluating the jet penetration depth, and these are summarized in Table (2.1).

Table 2.1 Correlations for the Jet Penetration Depth (Zhong et al., 2005)

Jet penetration correlations	References
$\dfrac{L_j}{d_j} = 821\left[\dfrac{(u_j - u_{mf})^2}{g d_p}\right]^{0.54}\left(\dfrac{\rho_g}{\rho_p}\right)^{0.67}\left[\dfrac{\rho_g d_p (u_j - u_{mf})}{\mu}\right]^{-0.34}\left(\dfrac{d_p}{d_j}\right)^{0.43}$	**Wu and Whiting (1988)**
$\dfrac{L_j}{d_j} = 26.9\left(\dfrac{u_j^2}{g d_j}\right)^{0.322}\left(\dfrac{\rho_g}{\rho_p}\right)^{0.325}\left(\dfrac{\rho_p u_j d_p^2}{\mu d_j}\right)^{-0.124}$	**Blake et al. (1990)**
$\dfrac{L_j}{d_j} = 26.47\left(\dfrac{\rho_g}{\rho_p - \rho_g}\dfrac{u_j^2}{g d_j}\right)^{0.293}\left(\dfrac{\rho_g u_j d_p}{\mu}\right)^{-0.1138}$	**Hong et al. (2003)**
$0.044\dfrac{L_j}{d_j} + 1.3 = 0.5\,\log(\rho_g u_j^2)$	**Zenz (1968)**
$\dfrac{L_j}{d_j} = \left(\dfrac{0.919 d_p}{0.0007 + 0.56 d_p}\right)\dfrac{u_j^{0.35}}{d_j^{0.3}}$	**Basov et al. (1969)**
$\dfrac{L_j}{d_j} = \dfrac{\pi}{4}\left(\dfrac{\rho_g}{\rho_p - \rho_g}\dfrac{u_j^2}{g d_j}\right)^{0.5}$	**Turner (1973)**
$\dfrac{L_j}{d_j} = 5.2\left(\dfrac{\rho_g d_j}{\rho_p d_p}\right)^{0.3}\left[1.3\left(\dfrac{u_j^2}{g d_j}\right)^{0.2} - 1\right]$	**Merry (1975)**
$\dfrac{L_j}{d_j} = 6.5\left(\dfrac{\rho_g}{\rho_p - \rho_g}\dfrac{u_j^2}{g d_j}\right)^{0.5}$	**Yang and Keairns (1978)**
$\dfrac{L_j}{d_j} = 15.0\left(\dfrac{\rho_g}{\rho_p - \rho_g}\dfrac{u_j^2}{g d_j}\right)^{0.187}$	**Yang and Keairns (1979)**
$\dfrac{L_j}{d_j} = 26.6\left(\dfrac{\rho_g u_j}{\rho_p \sqrt{g d_j}}\right)^{0.67}\left(\dfrac{u}{u_{mf}}\right)^{-0.24}$	**Hirsan et al. (1980)**
$\dfrac{L_j}{d_j} = 19.3\left(\dfrac{\rho_g u_j}{\rho_p \sqrt{g d_p}}\right)^{0.88}\left(\dfrac{u}{u_{mf}}\right)^{-0.54}$	**Knowlton and Hirsan (1980)**

The jet penetration depth or height is the length traveled by the disturbance associated with the jet injection (DeYoung., 2004). The correlations presented in the Table 2.1 were mostly derived from experiments by the associated authors. The jet penetration property is very important for designing operating conditions for jetting experiments. For instance, if the jet penetration were too large, large bubbles and possibly slugging would be observed. The experimental results show a dependence of the jet penetration depth on the nozzle diameter, particle density, static bed height and fluidizing gas flow rate.

2.3.3 Jet Half Angle

Looking back at Figure 2.3(b), it is shown for the case of a permanent flame, that the propagated jet is symmetric about an angle. This angle is known as the jet half angle, and it is a very useful simplification concept for calculating the bubble size. According to Merry (1975), the jet half angle can be represented by

$$\cot\theta = 10.4 \left(\frac{\rho_p d_p}{\rho_f d_o} \right)^{-0.3} \tag{2.5}$$

In order to fit newly available data ,Wu and Whiting (1988) recommended

$$\cot\theta = 8.79 \left(\frac{\rho_p d_p}{\rho_f d_o} \right)^{-0.236} \tag{2.6}$$

To relate the bubble size to the jet penetration depth, the following equation can be used

$$\theta = \tan^{-1} \left[\frac{D_B - d_o}{2L_j} \right] \tag{2.7}$$

A recent study done by Vaccaro (1997) showed that the jet half angle can be related to the two phase half angle where the solid particles are fed pneumatically into the fluidization column through the nozzle. It was mentioned earlier that jets enhance gas-solid contacting within the bed by entrainment, but this contact also results in the serious attrition of the particles by the acceleration and collision of the particles. In order to better quantify the jetting region, the jet half angle or expansion angle should be known, because it is an indication of the region spanned by the jet. Experimental results suggest that the jet half angle is affected by the operating pressure of the nozzle, the bed temperature, orifice size, and the jet velocity.

2.3.4 Interacting Jets

In configurations where there is more than one nozzle present in the fluidized bed. It is expected that jets would assume a different flow profile with increasing flow. This is shown for the upward pointing nozzles in Figure 2.4.
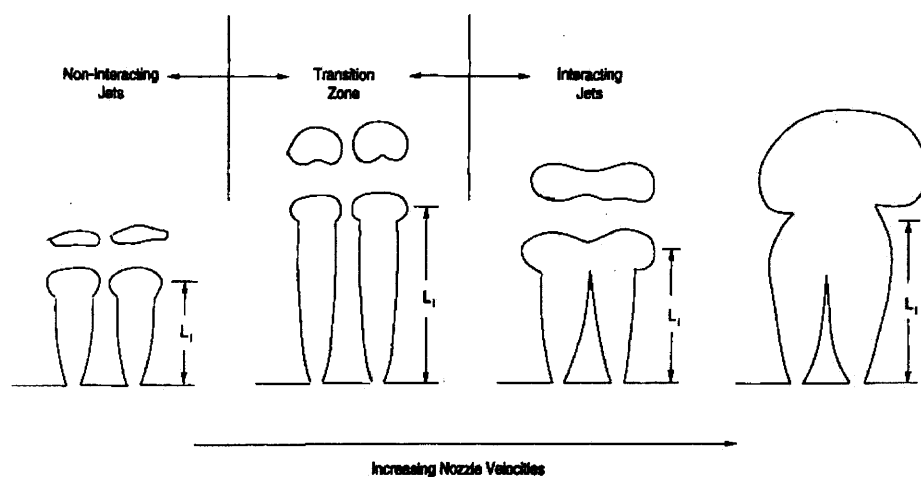

Figure 2.4 Interaction of multiple jets in a fluidized bed (Wu and Whiting, 1988).

For the double nozzles shown, initially the jets behave as non-interacting jets also known as separated jets, but as the velocities from the nozzles increase, they go through a transition phase and with high enough velocity, they coalesce (Guo et al. 2002). Jet coalescence was found to depend on the distance between the nozzles, and the operating conditions. Besides their application to fluidization, multiple nozzles have also been applied to grind particles (Tadashi et al., 2006). Here the operating pressure, the linear velocity at the nozzle, and the mass of raw material are the important parameters.

2.3.5 The Use of Internals in Fluidized Beds

Internals include tubes, baffles and other obstructions placed within the fluidized bed to better its performance. For example a process which requires large amount of heat transfer in the fluidized bed, may make use of immersed tubes to act as surface for heat exchange.

Internals such as baffles and internal tubes are very useful tools for impacting the gas solid contacting pattern in a fluidized bed. One such impact, is the control of the distribution and size of bubbles. It was shown by Jin et al. (1982) that the effect of baffles in the control of bubble size, was velocity dependent (Jin et al, 1982). At low velocities there are usually small bubble present which push upward through the baffle and collapse at the bed surface. However, at much higher gas velocities, the baffles are effective in breaking the larger and more frequent bubbles which emerge (Jin et al, 1982). There are many types of internals, each with its advantages and disadvantages when inserted within a fluidized bed. A pictorial representation of different internals and their uses is shown is Figure 2.5
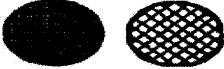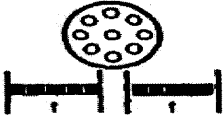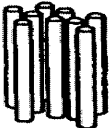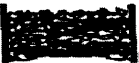
Category	Type	Configuration	Main features
Baffles	Wire mesh		1. Increase bubble splitting 2. Low erosion
	Perforated plate		1. Improve radial solids distribution 2. Increase bubble frequency
	Single- or multiple-turn plate		1. Enhance gas and solids exchange 2. Decrease elutriation 3. Improve radial bubble distribution
	Louver plate		1. Enhance gas and solids exchange 2. Decrease elutriation 3. Improve radial bubble distribution
	Ring		1. Improve radial voidage distribution 2. Enhance radial gas and solids mixing 3. Improve gas-solids contact efficiency 4. Suppress axial solids mixing 5. Increase conversion of ozone decomposition reaction
Tubes	Vertical banks		1. High heat-exchange coefficient 2. Low erosion phenomenon 3. Low scale-up effect
Packings	Station, irregular		1. Keep bubbles small and uniformly distributed 2. Reduce carryover of particles 3. Increase bed expansion 4. Increase chemical conversion 5. Impede solids motion
	Station, regular		1. Increase pressure drop 2. Increase solids holdup 3. Improve gas—solid contact efficiency
	Floating		1. Binary particles with different size and density 2. Larger particles float freely in the bed

Figure 2.5 Types of Internals and their uses (Yang, 2003).

The Figure 2.5 shows a pictorial view of tubes, packings and baffles, and outlines their applications. For example, station packings are used to increase pressure drop, solid hold up and gas contacting efficiency, while baffles can prevent bubbles from growing, continuously redistribute bubbles across the cross section of the bed, strengthen heat and mass transfer between the phases involved and decrease the rate of entrainment of solids (Yang., 2003). As shown in the figure, baffles may be in the form meshes, plates, and rings. Each design is tailored to a particular purpose. In the case of tubes, they are usually employed within the fluidized bed to improve heat transfer, although designing the right one for a process may in itself constitute a problem. Common associated problems include choice of optimal size, orientation, and tube spacing.

CHAPTER 3

JET ASSISTED FLUIDIZATION OF NANOPARTICLE AGGLOMERATES

3.1 Introduction

It is known that the agglomerates of nanoparticles present problems when they are fluidized conventionally without the use of some form of assistance. This is especially true for ABF type particles. For this reason, there is a lot of ongoing research regarding ways to better fluidize these materials. Several assisting methods such as sound assisted fluidization (Zhu et al. 2004), vibration assisted fluidization (Nam et al. 2004), the use of a rotating fluidized bed (Quevedo et al. 2006), fluidization in an oscillating magnetic field (Yu et al. 2005), and surface modification (Guo et al. 2006) have already been employed to this effect. In this work, we have successfully improved the fluidization behavior of several nanoparticle agglomerates via the assistance of a jet.

Jets have widely been studied in one form or another for different purposes. In fluidized beds, jets are generally employed to facilitate mixing, improve contacting of both solid and gas phases, improve heat and mass transfer and to break-down particles in to smaller sizes. In applications prior to this work, the jets were generated from orifices larger than 500 microns, and at velocities usually less than 100 m/s. By improving on the aforementioned limitations, it was possible to achieve very significant results in nanoparticle agglomerate fluidization.

3.2 Experimental Set-Up and Procedure

The experimental setup consisted of the fluid (nitrogen) source, the fluidization column, and the instruments for acquiring experimental data. A schematic of the experiment is shown in Figure 3.1. The fluid used for the experiments was dry nitrogen which was stored in a pressurized cylinder with an initial pressure of approximately 2500 psig. The cylinder is connected to a manifold which splits the flow from the cylinder. Two pressure regulators, each with a maximum pressure in the range of 140 psig were connected to the manifold, and their pressure rating were pre-regulated to 20 and 120 psig.
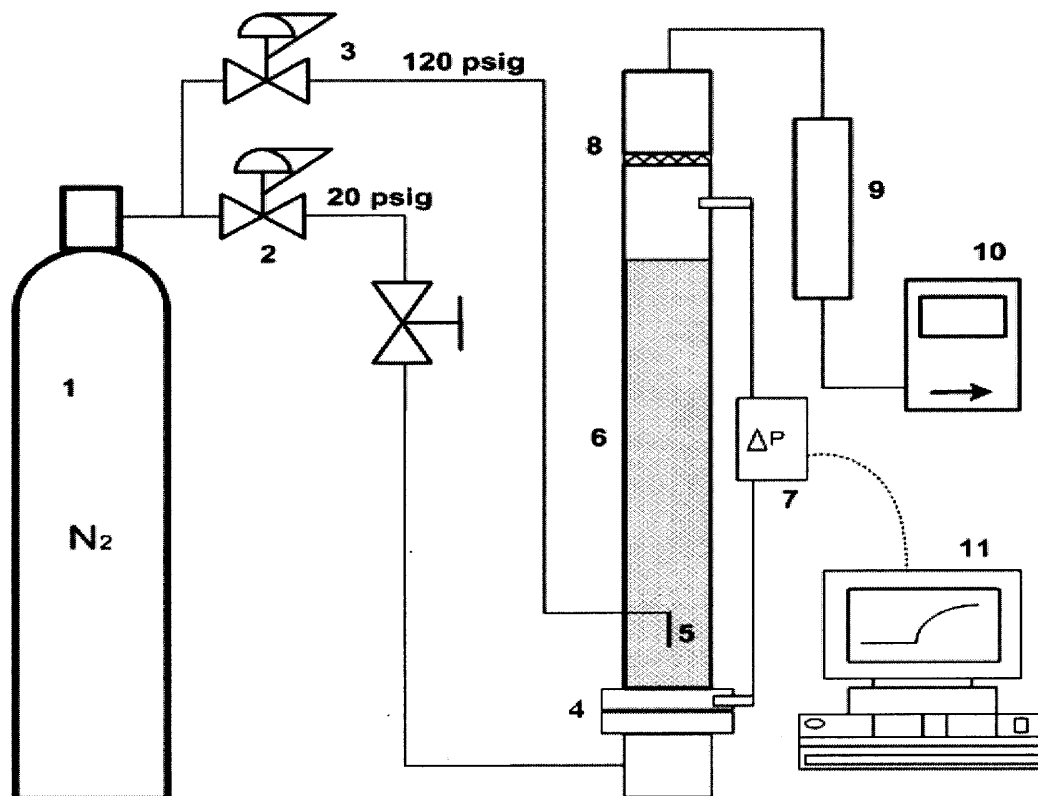
Figure 3.1 Schematic diagram of the experimental setup. (1) compressed dry N2 cylinder, (2) Pressure regulator for low pressure, (3) pressure regulator for high pressure, (4) Distributor, (5) micro-nozzle, (6) fluidization column, (7) differential pressure transmitter, (8) pre-filter, (9) HEPA filter, (10) flowmeter and (11) computer.

The low pressure line (20 psig) is equipped with a needle valve to control the flow rate of the fluid. This line feeds the fluid to the bottom of the column through the distributor plate, and into the bed. In this work this line is regarded as the "primary flow" line. The high pressure line (120 psig) has a globe valve equipped to it, which basically acts as an on-off switch. This line is connected to the nozzle(s), which are inserted through the side of the fluidized bed column at a predetermined height. The nozzles are located 4 inches above the distributor plate, and this line is referred to as the "secondary flow" line.

The fluidized bed column is made of cast acrylic plastic. The main section, which is cylindrically shaped, has an internal diameter of 3 inches and a thickness of 0.25 inches. The length of the column is adjustable up to a total height of 10 feet to accommodate the large bed expansion observed in some of the experiments. The adjustment is done, by simply removing the top section and interlocking it into an extension section.

The distributor is a sintered metal plate with 20 micron orifices. The open area is about 40% and it is has a thickness of a few millimeters. This plate is used to uniformly distribute the primary flow. Fluidization of the powder when just the primary flow is passing through the sintered plate is regarded as conventional fluidization. The top of the column is closed off with a copper tubing line leading out of it, and before this line, there is a wire mesh filter which acts to reduce the downstream concentration of elutriated particles. A HEPA capsule is connected outside the column before two mass flow meters which are used to measure the superficial gas velocity. It is important that none of the elutriated particles get in to the mass flow meters, otherwise they may become damaged.

Different sizes, orientation, and number of the nozzles were used during the experiments, and for each case the column was configured accordingly. These nozzles with orifice sizes ranging from 127 to 508 μm, and approximately 1 inch in length were obtained from Varian Inc. Once the experiment to be run was determined, the appropriate nozzle was selected and welded to the copper tubing connected to the secondary line. For a single, down pointing nozzle, the nozzle was usually inserted through the side of the column, and positioned 4 inches above the distributor plate. When facing upwards, the actual nozzle length is generally shorter, and its tip is about 8 inches from the level of the distributor plate. When multiple downward nozzles are used, they are symmetrically placed in the column with a 1 inch gap between them and at a 4 inch distance from the distributor. An illustration of the different configurations used in this work is shown in Figure 3. 2.

(1) Nozzle, (2) Distributor Plate, (A) Single downward nozzle, (B) Single upward nozzle
(C) Multiple downward nozzles
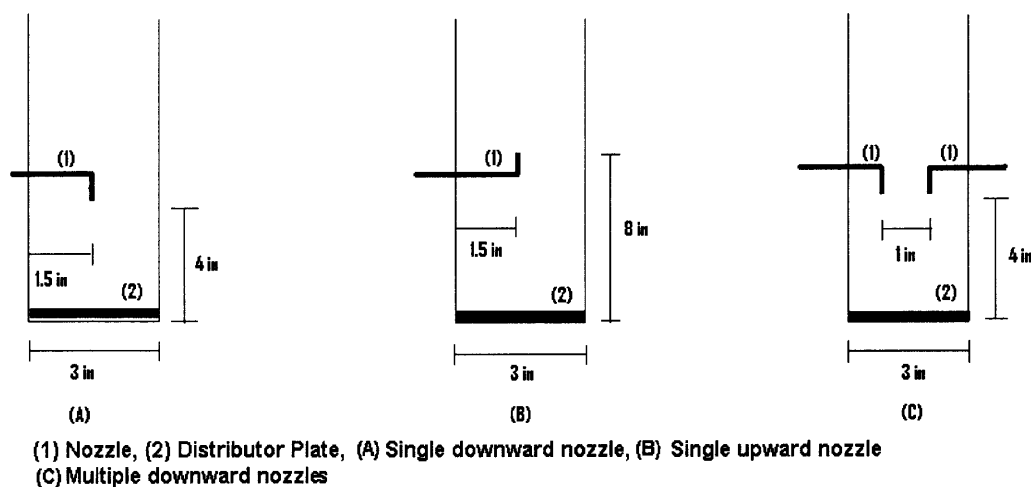
Figure 3.2 Configurations of nozzles.

Generally, experiments were done using different nozzles, operating at different pressures to alter the gas velocity through the jet, and using multiple nozzles, to exceed

flow restrictions. Table 3.1 below shows the properties of the different nozzles that were tested.

Table 3.1 Properties of the Nozzles

Size	Color	Nozzle	Pressure	Flow rate	Velocity
μm	Code	#	psig	lpm	m/s
127	Red	1	120	0.4	526
177.8	Black	1	120	1	671
228.6	Gold	1	120	1.3	528
254	Blue	1	120	1.5	493
508	Green	1	1-120	15	1233

The table shows the sizes of the nozzles that were used in the jet assisted fluidization experiments. Their sizes ranged from 120 microns to 508 microns, and the jet velocity ranged from 493 to 1233 m/s. It was observed that while operating at a higher pressure, the fluidization quality in terms of homogeneity could be negatively affected due to the relatively large flow rates from the nozzles. This observation was most prominent with the large nozzles. For the smaller nozzles, although their jet velocities could be in the order of 500 m/s, their contribution to the total flow rate which was measured after the column was still relatively low.

The pressure and velocity through the nozzle is a representation of how much momentum the flow carries. This flow dissipates by shearing and entraining the particles in its immediate environment along the axis of the disturbance generated by the propagated jet.

After the HEPA filter, the line is split in two, to allow the measurement of the fluid flow rate, by two Omega mass flow meters (model FMA 1700/1800 series) with ranges 0 to 5 and 0 to 20 liters per minute. The flow meters were located at the exit of the column to ensure that the measurements of the superficial gas velocity were taken at near atmospheric conditions. Generally, for low flow experiments, the lower range mass flow meter was used.

Pressure taps were located right above the sintered distributor plate and before the wire mesh filter at the exit of the column to measure the pressure drop across the column. These taps were connected to a differential pressure transmitter, sensitive to pressures as low as one thousandth of an inch of water. Depending on the pressure drop of the fluidized bed, which was usually in the range of 0 to 5 inches of water, an appropriate transmitter was selected. The pressure transmitter was connected to a Cole Palmer digital display (model 93482-02), which can be linked to a computer using a RS-232 data cable. The software used to communicate between the computer and the display was MeterView software.

Some of the experiments were carried out with the aid of internal plates, which were perforated with a near symmetric distribution of holes on their surface. The plates were made from acrylic plastic, with a diameter of approximately 3 inches, and thickness of about 0.25 inches. The plates that were used differed in the size of their holes, which ranged from 0.27 to 0.43 inches, and one of the plates had no center holes in order to further alter the flow pattern. In the experiments, the plates were located 12 inches above the distributor plate, the nozzle was then located 4 inches above the plate, and the nanopowder to be studied was fed from the top such that it sat on the plate. Figure 3.3

shows the types of plates that were used. The two "type A" plates had holes of either 0.275 in, or 0.433 in respectively, while the type B plate had holes of the size 0.354 in, with no hole in the center.

Figure 3.3 Types of Perforated Plates.
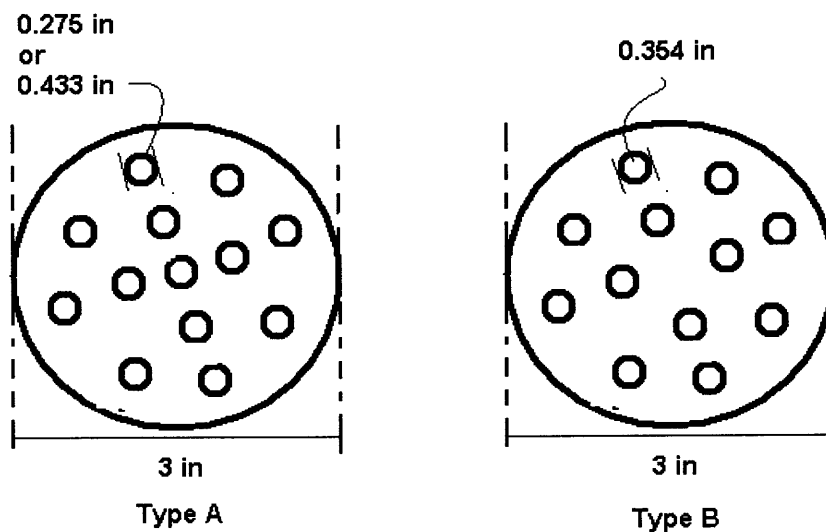
The powders that were studied in this work are Degussa Aerosil R974, Aerosil A90, Aerosil A200, Aeroxide TiO_2, and Aeroxide Alumina C. The different powders have different jet processing rates as will later be shown in the bed height vs. jet processing time plots, and hence behave differently under the influence of the jet. Table 3.2 summarizes the properties of the different powders.

Table 3.2 Properties of the Powders

Powder	Grade	Used Name	Property	Fluidization Behavior	Primary Particle size, [nm]	Sieve Size μm	Tapped Density [kg/m³]
Aerosil R974	Commercial	R974	Hydrophobic	APF	12	500	50
Aerosil A90	Commercial	A90	Hydrophilic	ABF	20	850	80
Aerosil A200	Commercial	A200	Hydrophilic	APF	12	850	50
Aeroxide TiO₂ P25	Commercial	TiO₂	Hydrophilic	ABF	21	500	130
Aeroxide TiO₂ P25	Process	Raw TiO₂	Hydrophilic	ABF	21	500	130
Aeroxide Alu C	Commercial	Alu C	Hydrophilic	ABF	13	850	50

Based on conventional fluidization alone, the powders can be divided into ABF (Agglomerate Bubbling Fluidization) and APF (Agglomerate Particle Fluidization). ABF type powders are difficult to fluidize, show relatively low bed expansion, and are typified by the bubbling behavior observed upon reaching fluidization, while APF powders show smooth, homogeneous fluidization without bubbles and relatively high bed expansion. In terms of surface properties, all the powders that were used with the exception of R974 are hydrophilic. It should be also noted that R974 is a modified form of A200, and this modification alters both the conventional and jet assisted fluidization behavior of the powder. For the TiO_2, the process grade refers to samples that were taken directly from the production lines, while the commercial grade (all powders) is the form retailed to customers. The studied nanoparticle agglomerates have primary particle sizes in the range of the about 12 to 20 nm which coalesce into "simple" agglomerates and these simple agglomerates form larger "complex" fractal structured agglomerates of about 200-300 microns.

At the start of each of experiment, the powder was pre-sieved with a 500 or 850 μm mesh sieve to remove large agglomerates present in the powder. The powder was then weighed and poured into the column. Prior to pouring in the powder, the column was usually sprayed with an electrostatic spray to reduce the amount of electrostatic charge which usually built up within the column. In many of the experiments the dry nitrogen was first passed through a tank of ethyl alcohol; the addition of a very small amount of alcohol vapor to the fluidizing gas was very effective in reducing the electrostatic charge build-up.

In the conventional mode of fluidization, the sieved bed of particles is fluidized with flow from the primary line alone, while in the jet assisted fluidization, the primary flow is first adjusted to allow minimal fluid flow through the bed. Next, the jet is turned on, and then the primary flow is progressively increased with data points for gas velocity, bed height, and pressure drop during each increment of the flow rate being recorded. Also the MeterView software was configured to continuously monitor the pressure drop value across the bed.

3.3 Results and Discussion

In comparison to previous works, which used larger nozzles and lower jet velocities to fluidize Group B and D powders (Geldart classification), this work scaled down the size of the orifice, operated at high pressure, increased the jet velocities through the nozzles, and coupled the jet flow with flow through the distributor. These modifications generally resulted in an unprecedented behavior of all the particles that were studied with respect to

their fluidization. In all cases, the results showed a successful and improved fluidization behavior of the nanoparticle agglomerates.

With regard to the jet assisted fluidization, there are many correlations available in the literature for predicting the jet penetration depth. These equations have already been previewed in Table 2.1, and Table 3.3 shows the values obtained after the insertion of the necessary parameters into the appropriate equations used for the purpose of this work.

Table 3.3 Theoretical Values Obtained from the Correlations in Table 2.1

Nozzle Code	Red	Black	Gray	Blue	Green
Nozzle Size, [μm]	127	177.8	228.6	254	508
Reference	Lj, [cm]	Lj, [cm]	Lj, [cm]	Lj, [cm]	Lj, [cm]
Turner (1973)	28.15	42.66	38.06	37.46	132.49
Basov et al (1969)	0.38	0.52	0.57	0.60	1.35
Merry (1975)	1.25	2.00	2.39	2.60	8.09
Wu and Whiting (1988)	39.04	51.38	54.65	56.69	114.94
Yang and Keairns (1978)	234.01	353.21	315.15	310.18	1097.08
Yang and Keairns (1979)	4.07	5.36	6.02	6.39	15.81
Hirsan et al (1980)	22.31	32.85	33.06	33.87	99.25
Knowlton and Hirsan (1980)	17.36	25.97	24.21	24.18	79.85
Blake et al (1990)	11.65	17.31	18.70	19.63	55.14
Hong et al. (2003)	12.96	18.44	19.67	20.52	51.64
Zenz (1968)	0.42	0.63	0.76	0.82	2.10

The values in Table 3.3 were obtained for R974, with a bulk density of 33.24 kg/m^3. The properties related to the jet are already tabulated in Table 3.1. Most of the

equations used are related to the modified Froude number, which is a dimensionless quantity relating the density of the powder, density of the fluid, diameter of the nozzle's orifice, and the jet velocity. Other independent properties include the superficial gas velocity, static bed height, and the diameter of the particle. Careful examination of the values obtained suggests that some of the correlations are not suitable for the purpose of this work. An example would be the high jet penetration depth values (>230 cm) predicted by the Yang and Keairns (1978) correlation. Using the Red (127 μm) nozzle as reference, visual observation suggests that the jet penetration depth should not be larger than 10 cm, and correlations which suggests otherwise are not appropriate for the purpose of this experimental investigation. The differences in the obtained values from the correlations stem from the type and properties of particles studied, properties of the jets, and the range of data available for the correlation.

The jet penetration depth is important for this work, because in most of the experiments, the nozzle(s) was oriented downwards towards the distributor plate, and a large jet penetration depth would imply that the powder is continuously being bombarded against the distributor plate. This event may lead to the clogging up of the distributor plate, which would in turn affect the uniformity of the flow through it, and consequently the fluidization behavior.

3.3.1 Jet Assisted Fluidization of Aerosil R974

The fluidization behavior of R74 as shown in Table 3.1 is characterized as APF, which implies that when it is fluidized conventionally, high expansion and homogeneity are expected. In this work, we fluidized different masses of Aerosil R974 conventionally and

under the influence of a jet. The result from the conventional fluidization and jet assisted

fluidization of 3 different amounts (9.5 g, 13 g, and 20 g) of R974 is shown in Figures 3.4

and 3.5.
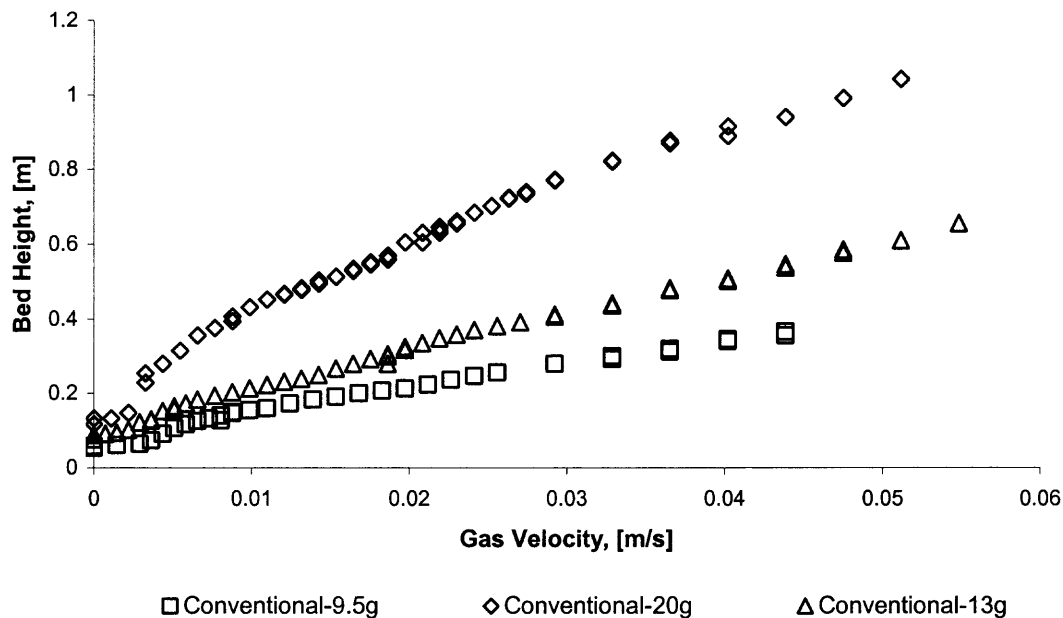
Figure 3.4 Bed height vs. gas velocity for conventional fluidization of 9.5g, 13g and 20g of R974.

Figure 3.4 shows the effect of the conventional upward flow of gas on different

amounts of R974. The trend represented in the figure is expected, and is well in line with

the experimental results found in literature. For example, at a gas velocity of 0.025 m/s,

Zhu et al. (2005) and Yu et al. (2005) reported a bed expansion ratio of 4-5 times the

initial bed height. For the data shown in Figure 3.4, the initial bed height for the 9.5 g, 13

g and 20 g powder were 0.053 m, 0.077 m, and 0.116 m, respectively which corresponds

to bed expansion ratios of 4.64, 4.88, and 5.6, respectively at a gas velocity of 0.025 m/s.

The results from the conventional fluidization can then be compared to the jet assisted
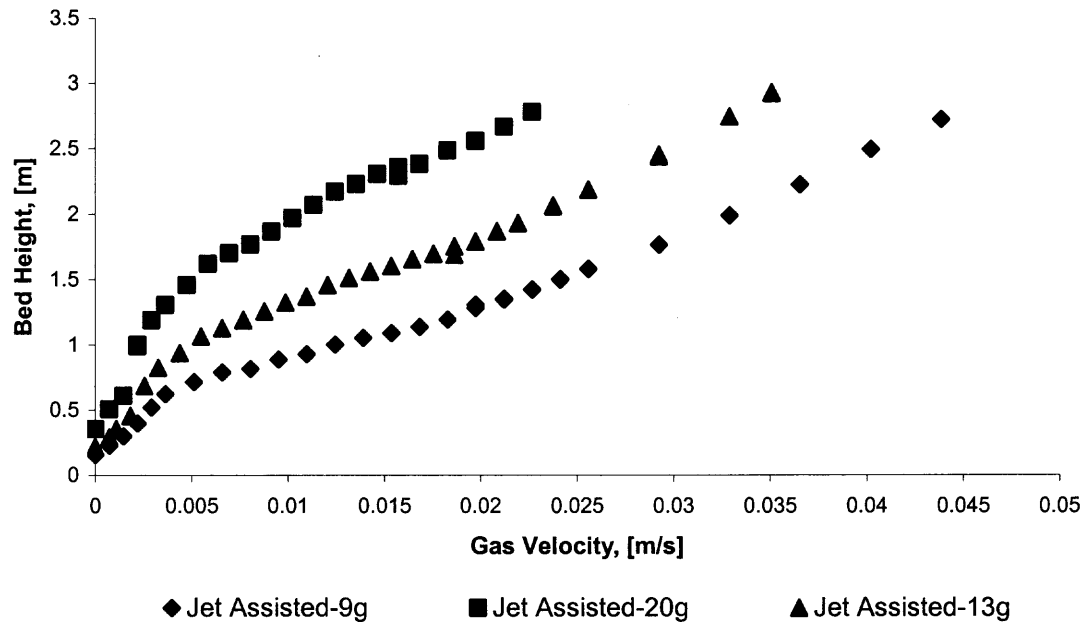
method which is shown in Figure 3.5.

Figure 3.5 Bed height vs. gas velocity for jet assisted fluidization of 9.5g, 13g and 20g of R974.

Figure 3.5 shows the effect of the jet assisted method on the different amounts of powder that were already fluidized conventionally and represented in Figure 3.4. The first run of the experiments were done with 20 g of R974 agglomerates, and in the jet assisted fluidization of the powder, it had expanded beyond the capacity of the 10 feet column which led to an early termination of the experiment. This is illustrated in Figure 3.5 by the square points corresponding to 20g of R974, whose fluidization was stopped at about 0.025 m/s. The powder was then scaled down to 13 g and finally to 9.5 g in order to accommodate the phenomenal expansion caused by the jet's influence.

In comparing the conventional method with the jet assisted method, it is seen that for the 20 g powder, at a gas velocity of 0.025 m/s the powder was dispersed to approximately 5.6 times its initial bed height by the conventional method which pales in comparison to the 27 times the initial bed height achieved by the jet assisted mode. For a

comparison at a higher gas velocity, which was possible for 9.5 g of R974 (without overflowing the column), it is seen that at a gas velocity of 0.045 m/s, the bed of R974 agglomerates was dispersed to about 7 times its initial bed height, while for the jet assisted mode, it was possible to disperse the same powder, at the same velocity to about 51 times the initial bed height, which is a dramatic increase in the dispersion of the powder.

Also observed and already corroborated by previous experiments was that R974 begins to bubble at around 2.5 cm/s with conventional fluidization, but under the influence of the jet, bubbling was not observed for R974 for any of the experiments. After all flow was shut off, and the bed was allowed to settle, the final settled bed height was higher than the initial bed height, which directly implied that the jet was not just acting to disperse the particles but also to lower their density and to break the larger agglomerates. Visual inspection also showed that the powder appeared fluffier after processing with the jet and the bulk density had been reduced.

The minimum fluidization velocities with regards to the 9.5, 13 and 20 g of R974, under both conventional and jet assisted fluidization are shown, in Figures 3.6 to 3.8
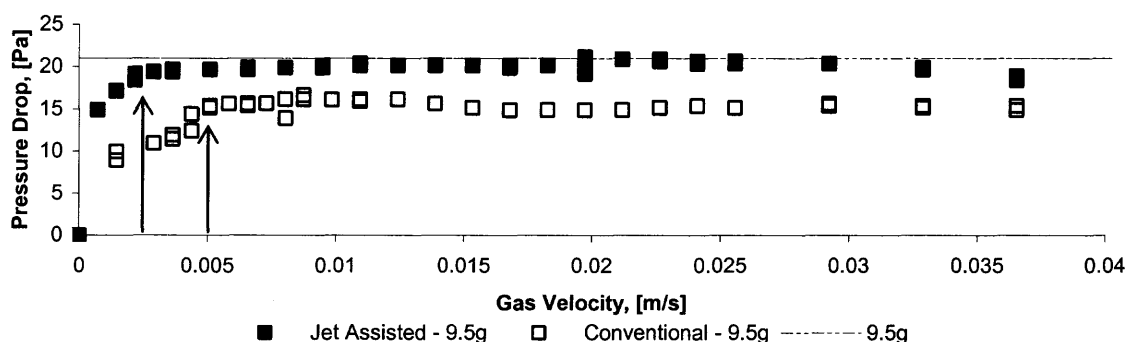
Figure 3.6 Comparison of the pressure drop for conventional and jet assisted fluidization with gas velocity for 9.5g R974.
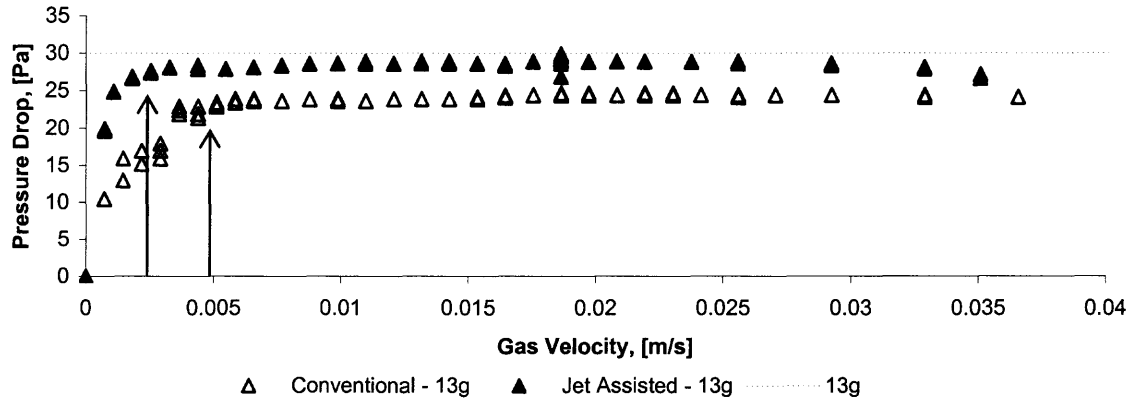
Figure 3.7 Comparison of the pressure drop for conventional and jet assisted fluidization with gas velocity for 13g R974.
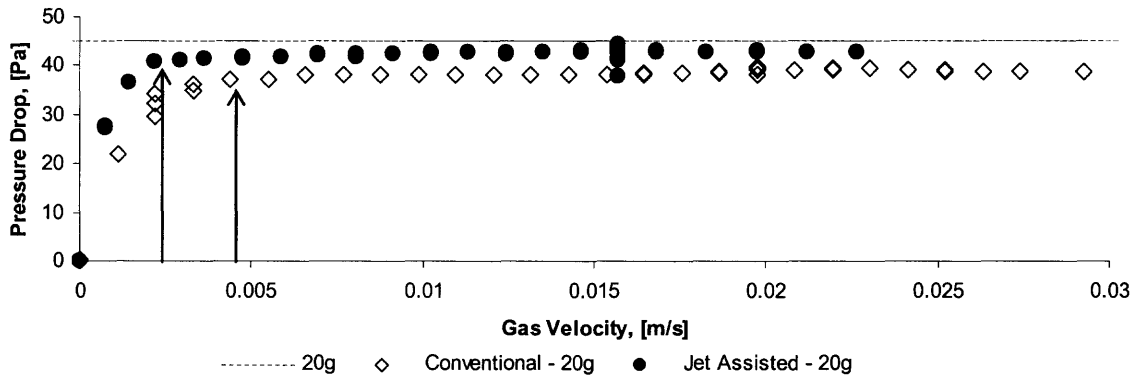
Figure 3.8 Comparison of the pressure drop for conventional and jet assisted fluidization with gas velocity for 20g R974.

As mentioned earlier, the minimum fluidization velocity (u_{mf}) represents the lowest velocity at which the bed of powder is suspended by the upward flow of the gas. The u_{mf} is indicated by the vertical upward pointing arrows in Figure 3.6-8, and at velocities greater than the u_{mf}, the pressure drop is seen to be relatively constant. For the different amounts of powder, the observed u_{mf} was 0.005 m/s for conventional fluidization and when the fluidization is assisted by the jet, the u_{mf} drops to 0.0025 m/s. Compared to previous works, Nam et al. (2004), Yu et al. (2005) and Zhu et al. (2005) reported a minimum fluidization velocity in the range of 0.003-0.004 m/s as their

conventional fluidization results for R974. The drop in u_{mf} in the jet assisted method is supported by the fact that under the jet assisted fluidization, the momentum contributed by the jet, improves mixing and breaks down the larger agglomerates which hinder smooth fluidization.

Also from Figures 3.6-3.8, the horizontal lines represent the actual weight of the bed of particles that the drag needs to support. It is seen in the plots that under conventional fluidization, the total suspension of all the bed particles is never achieved. This may due to agglomerates that settle at the bottom, and also slow moving or static powder at the wall of the fluidization column. In the case of fluidization under the influence of the jet, it is seen that the pressure drop just about equals the weight of the bed (per unit area) for the different masses of powder that were used. This improvement is due not only the fact that better contacting and mixing is achieved with the use of the jet, but also that the jet breaks down the larger agglomerates which settle at the bottom of the bed as well.

For the cases where the jet was applied, it is seen from the figures that at higher velocities the pressure drop starts to decline. Generally, this is an indication of elutriation of powder from the surface of the bed, which is common to both conventional and jet assisted fluidization. The main difference in the jet assisted fluidization of the different masses of powder lies in the time it takes to process each different amount of mass of powder, i.e., the time it takes until the bed expansion begins to level off. A representation of the jet processing time for 9.5 g, 13 g, and 20 g of R974 is shown in Figure 3.9.
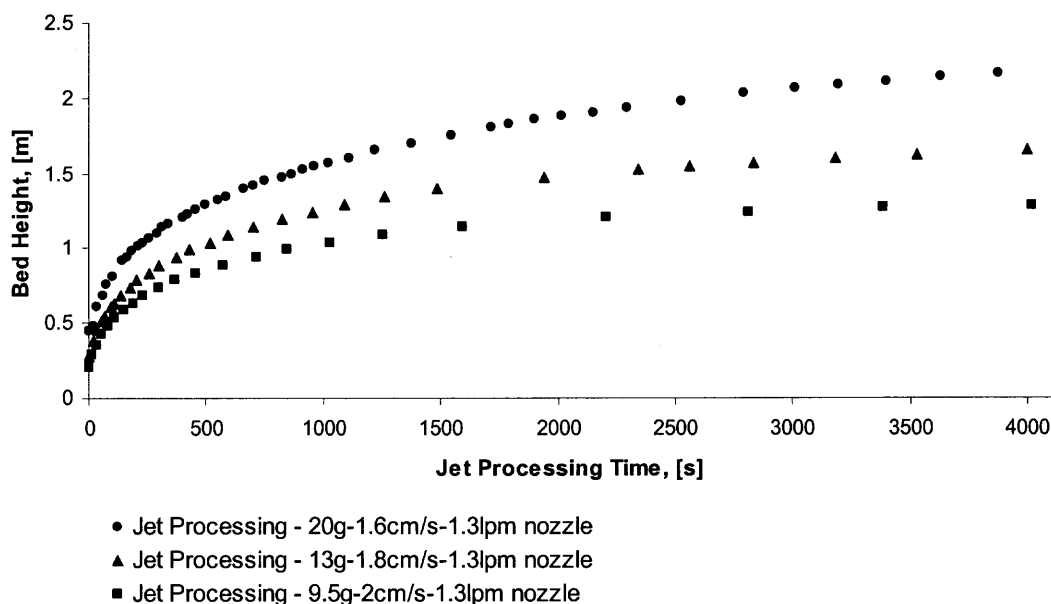
Figure 3.9 Jet processing of 9.5 g, 13 g, and 20 g of R974 with a 228.6 μm nozzle.

In the 4000 seconds window shown in Figure 3.9, it is seen that, the powder gets processed for all the cases, despite the difference in mass in each of the runs. It also shows that the time needed to process the powder is related to the mass of powder which is being processed. This can be clearly seen from the slope of each curve in the figure which levels off at different times. The processing speed is such that it decreases with the mass of powder.

To further demonstrate the effect of the micro nozzle jets on the fluidization behavior of R974, it was used to process an un-sieved version of the powder. Figure 3.10 shows the fundamental difference between a pre-sieved and an un-sieved version of R974 and the effect of processing the un-sieved powder with a micro nozzle.
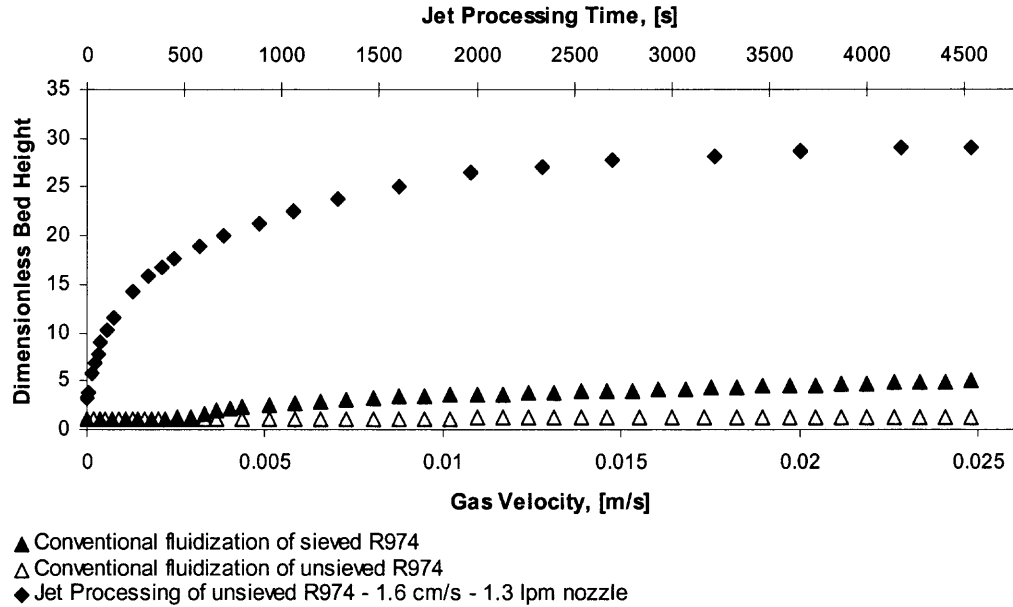
Figure 3.10 Effect of processing of un-sieved R974.

Unsieved R974 does not expand much when fluidized conventionally. When compared to the 5 times expansion at 0.025 m/s obtained when pre-sieved with a 500 μm mesh sieve, it only expands about 1.5 times its initial bed height. This is largely due to the large clusters of agglomerates present. However, by using the micro nozzle jet to break down these huge agglomerates, it becomes possible to get expansion up to 30 times and even more if the flow is further increased. The upper abscissa axis shows the 4500 seconds window which represents the processing speed of the unsieved R974 to an expansion height of 30 times its initial bed height.

3.3.2 Jet Assisted Fluidization of A200

The fluidization behavior of A200 is also classified as APF (Agglomerate particle fluidization), but unlike R974 which is a modified version of A200, A200 is hydrophilic. A200 generates a significant amount of electrostatic charge which tends to affect the

quality and homogeneity of its fluidization despite the use of the electrostatic reduction spray or the alcohol vapor.
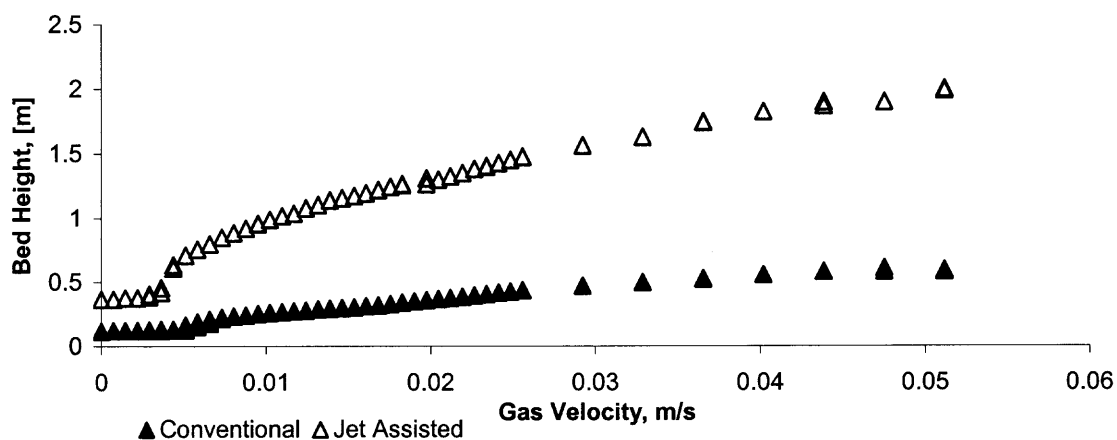
Figure 3.11 Comparison between jet assisted and conventional fluidization of A200.

Figure 3.11 shows the effect of increasing gas velocity on the fluidization behavior of 15.5 g of A200 for both the conventional mode and the jet assisted mode using the 1.3 lpm nozzle. From the figure, it is apparent that at a flow of 0.05 m/s, the bed of A200 particles had expanded approximately 5 times its initial bed height for the conventional mode, which is much lower than the 17 times bed expansion achieved under the assistance of the micro nozzle jet.

For the conventional case, bubbling was observed around 0.04 cm/s but it was not observed during operation with the jet. After fluidization with the micro nozzle, and after all of the gas flow was turned off, the final bed height was approximately 3 times the original bed height, signifying that the agglomerates were changed by the action of the micro jet.

After passing nitrogen through the column for some time, the amount of electrostatic charge in the column starts to build up, and this in turn affects the fluidization behavior of the powder. In Figure 3.12, the vertical arrow points
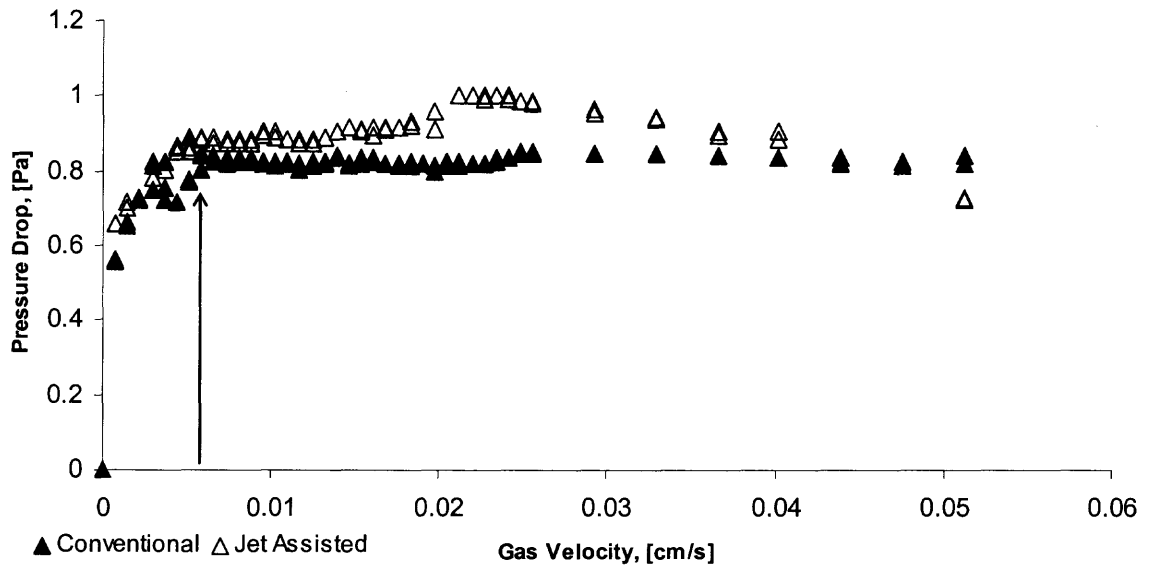
Figure 3.12 Comparison of pressure drop vs. fluidization gas velocity for both conventional and jet assisted fluidization of 15.5g of A200.

towards the minimum fluidization velocity of the pressure drop curve, and this was determined to be 0.006 m/s for both the jet assisted and the conventional cases. It is also shown in the figure that more A200 is being suspended under the influence of the jet (higher pressure drop), but with progressive increase in the gas velocity this value starts to drop. In this particular case, the decline observed in the pressure drop while using jet was due to the erratic behavior caused by the build up of electrostatic charge within the column at the higher velocities.

3.3.3 Jet Assisted Fluidization Alu C

The fluidization behavior of Alu C is classified as ABF (Agglomerate bubbling fluidization), which implies that very slight bed expansion and mostly bubbling type fluidization should be expected. Figures 3.13 and 3.14 show the observations that were made for conventional and jet assisted fluidization of the powder.

Figure 3.13 Effect of gas velocity on bed expansion in the conventional fluidization of 22 g Alu C.
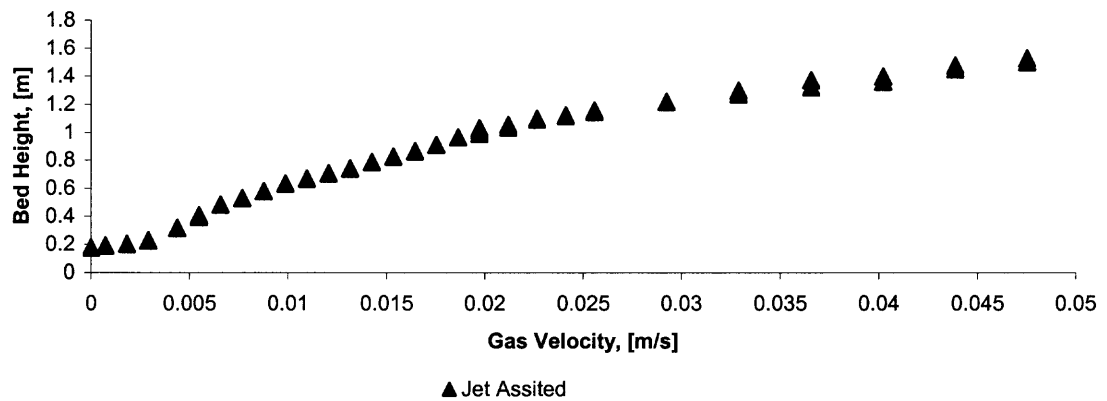
Figure 3.14 Effect of gas velocity on bed expansion in the jet assisted fluidization of 22 g Alu C.
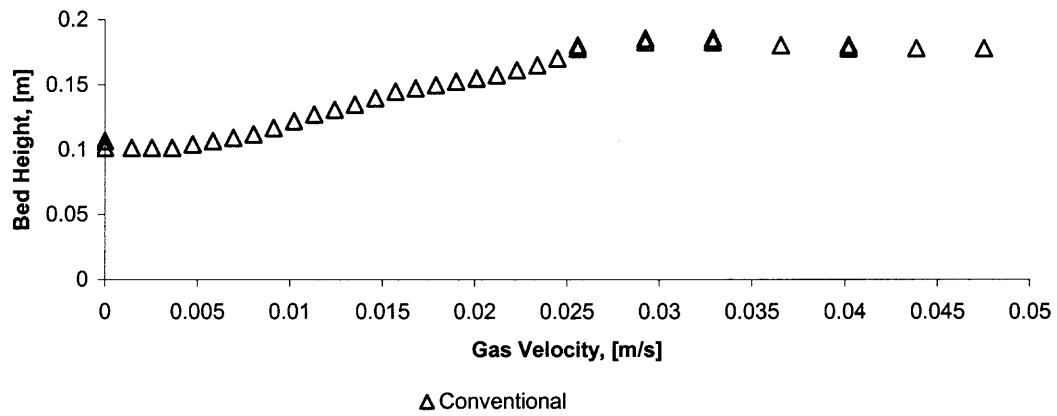
It can be seen in the plot that under the conventional flow of gas alone, the bed expansion at 0.05 m/s is about 1.6 times the original bed height, while for the jet assisted case, the bed expanded up to 14 times under similar operating conditions. Not shown is the minimum bubbling point which was observed at 2.9 cm/s for the conventional mode and 3.3 cm/s for the jet assisted. Despite the presence of slight bubbles, the bed still continued to expand in the jet assisted mode, and upon de-fluidization after the action of the jet, the observed final bed height was 1.7 times the original. The effect of the gas velocity on the pressure drop for the respective modes is shown is Fig 3.15.
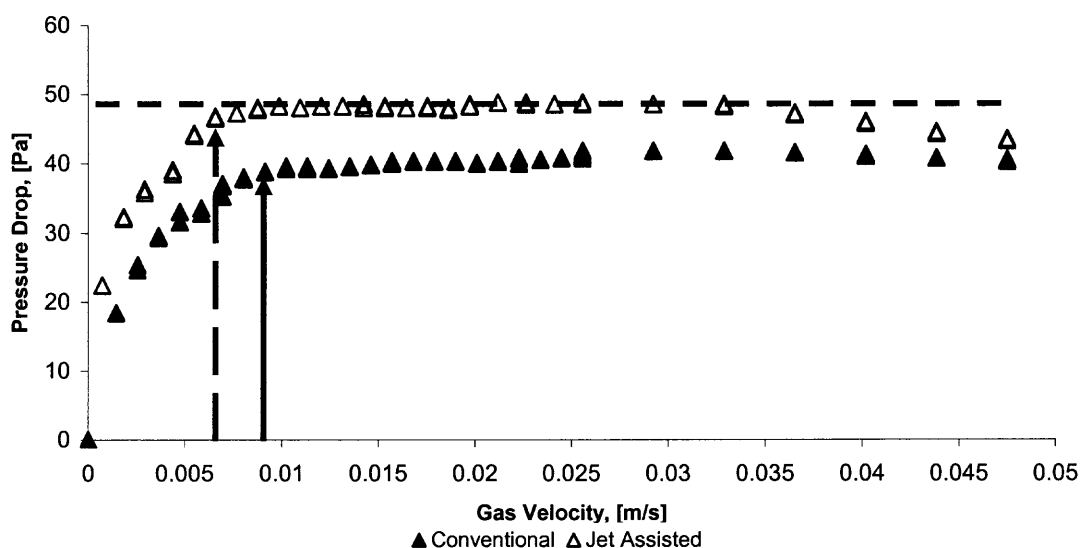
Figure 3.15 Comparison of pressure drop with respect to gas velocity of the conventional and jet assisted fluidization of 22g Alu C.

The vertical arrows represent the points at which the bed of Alu C particles become suspended (fluidized), and these corresponds to 0.0055 m/s and 0.008 m/s for the jet assisted and the conventional fluidization modes, respectively. It is also obvious that under the conventional flow of gas, not all the powder is suspended, but with the

increased contacting, mixing and agglomerate break-up action of the jet, it was possible to suspend almost the entirety of the bed of powder, as represented by proximity of the curve for the jet assisted method to the horizontal broken line which represents the actual weight of the bed per unit area. However, at high velocities, and after prolonged fluidization periods, elutriation and electrostatic charge build up with the column still posed a problem as seen by the decrease in the pressure drop.

3.3.4 Jet Assisted Fluidization of TiO$_2$

The fluidization behavior of TiO$_2$ was examined and compared under both conventional and jet assisted fluidization. Unlike the powders already presented, TiO$_2$ is much denser, and its conventional fluidization shows little or no bed expansion. The process grade TiO$_2$ (Raw TiO$_2$) however, behaves slightly better under the conventional fluidization mode. Since TiO$_2$ is known to be very difficult to fluidize, the effect of the jet on the fluidization of TiO$_2$, was studied to a greater detail compared to the powders already presented above.

Figure 3.16 presents the fluidization results for both the commercial and process grade of TiO$_2$. For each powder, 61 grams was pre-sieved using a 500 μm mesh sieve before it was fluidized either conventionally or with the aid of the jet using the 1.5 lpm nozzle. It should be noted that for the same mass, the Raw TiO$_2$ is initially 1.3 times the height of the commercial grade, making it the more porous of the two grades (lower bulk density). When the powders are fluidized conventionally, at a velocity of 0.04 m/s the
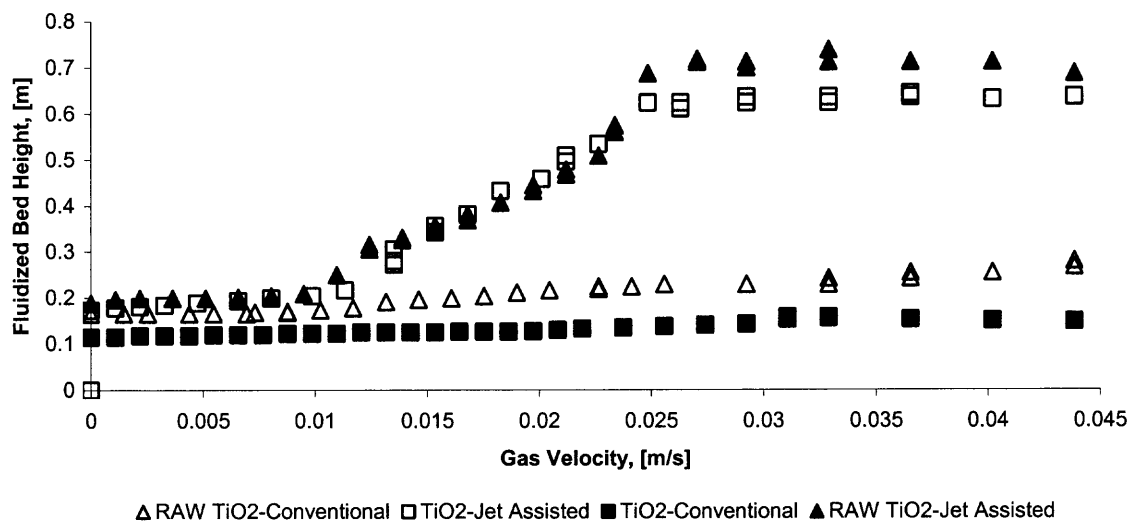
Figure 3.16 Bed Height as a function gas velocity during the fluidization of TiO_2 and Raw TiO_2

commercial grade expands to about 1.3 times its original bed height, while the process grade expands to about 1.6 times. By assisting the process with the micro nozzle jet, the bed expansion values are increased from 1.3 to 6 for the commercial grade and 1.6 to 4 times for the process grade TiO_2, but the final bed height of the RAW TiO_2 still exceeded the commercial grade. After the termination of all flow, the bed height was 1.3 times the original bed height for Raw TiO_2, and 1.4 for TiO_2 (Commercial grade).

TiO_2 is a very typical ABF powder, in the sense that once it reaches fluidization it starts to bubble, and it shows little or no bed expansion. This behavior was also reported by Zhu et al. (2005). However, by assisting its fluidization with the micro nozzle jet, it was possible to fluidize the powder homogenously, and attain the high bed expansion common to an APF powder. As for Raw TiO_2, although it showed little bed expansion under conventional fluidization, its behavior was still somewhat smooth, and by augmenting fluidization of both powders with the jet, a more homogeneous APF like powder behavior was observed as indicated by the higher bed expansion values.

Taking another look at Figure 3.16, the curves for the jet assisted fluidization can be divided into three segments. The first horizontal segment (0-0.01 m/s) shows that the bed height does not respond to flow rate. In this segment channeling and spouting is mostly observed. The next segment is an inclined segment (0.01-0.025 m/s), where the bed responds to flow rate under the influence of the jet, and in the final horizontal segment little bed expansion is also observed. Further increase in the flow rate in this segment leads to the generation of bubbles, and unsteadiness of the bed surface.

The next question was how much of the powder was suspended under the action of the micro nozzle jet for both commercial and process grade TiO_2, and this is addressed by Figures 3.17 and 3.18.
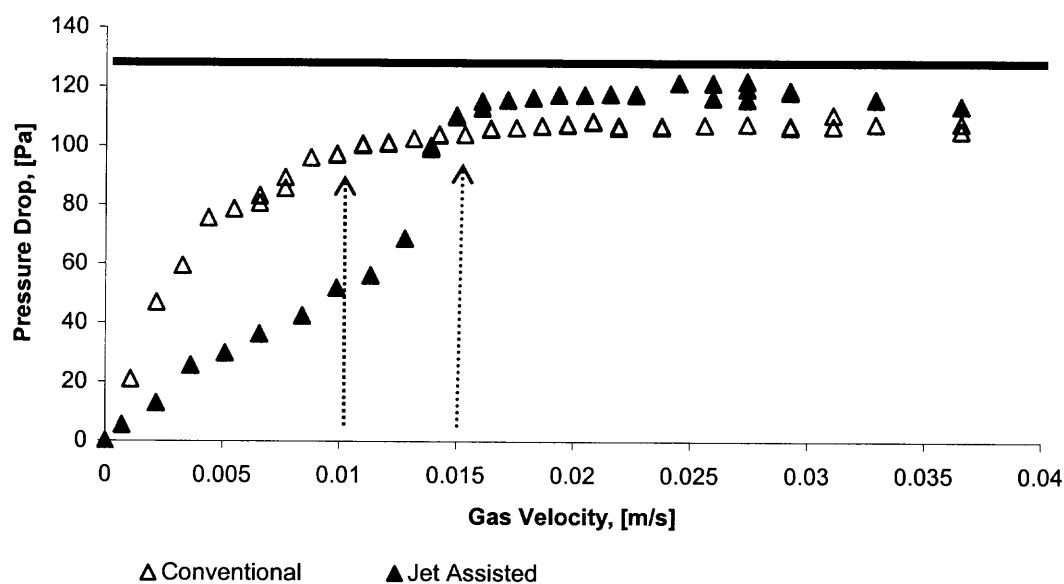

Figure 3.17 Pressure drop as a function gas velocity during the fluidization of TiO_2.
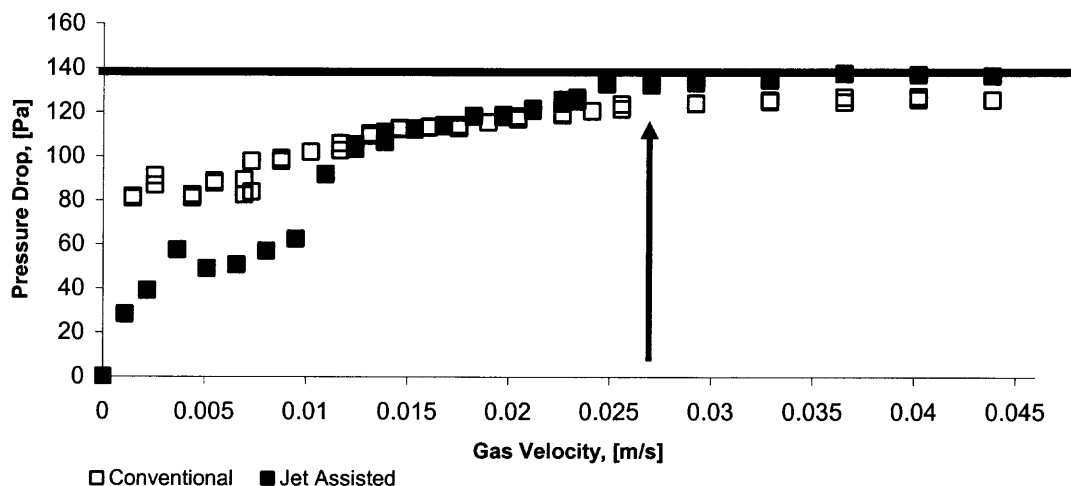
Figure 3.18 Pressure drop as a function gas velocity during the fluidization of RAW TiO$_2$.

The Figures 3.17 and 3.18 represent the behavior of the pressure drop in response to the gas velocity for a mass of 61 g for both grades of TiO$_2$. During the jet assisted fluidization, the 1.5 lpm nozzle was used. From the figures, it can be seen that the u$_{mf}$ for TiO$_2$ is approximately 0.01 m/s when fluidized conventionally and 0.015 m/s when fluidized with the jet, while for Raw TiO$_2$, the value is 0.025 m/s for both cases. It can also be deduced that for both grades of powder the jet assisted fluidization outperforms the conventional fluidization with respect to the volume of powder suspended. Comparing both powders, their jet assisted fluidization has a pressure drop closer to actual weight of the bed per unit area which is shown by the proximity of the pressure drops value (after the u$_{mf}$) to the horizontal line (weight of bed/unit area) compared, to their conventional fluidization. After obtaining these results, the jet assisted fluidization of the commercial grade TiO$_2$ was further explored. The next experiment was done to determine the effect of fluidizing TiO$_2$ under a reduced nozzle pressure and consequently a reduced momentum. Figure 3.19 summarizes these findings.
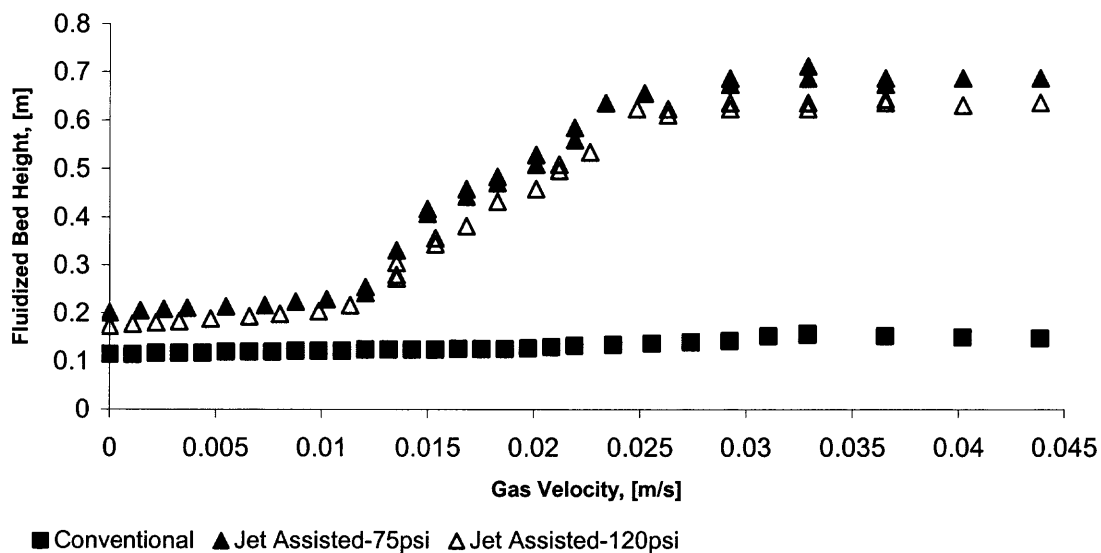
Figure 3.19 Effect of reduced pressure on the jet assisted fluidization of TiO_2.

The effect of pressure on the jet assisted fluidization of TiO_2 powder was studied

for 2 operating pressures (75 and 120 psig) with a (blue) 254 μm orifice nozzle. Under

these nozzle conditions, 60 g samples of TiO_2 were processed and fluidized. Figure 3.19

compares the results for the jet assisted mode with the conventional fluidization of TiO_2

at 120 psi. The jet assisted fluidization curves were found to be very similar, with regards

to their shape and bed height values. At a velocity of 0.04 m/s, it is clearly seen that the

jet assisted fluidization performs better than the conventional fluidization mode with a

bed expansion of about 6 times the initial bed height compared to the conventional mode

which yielded only 1.3 times the initial bed height. It was also observed that the final bed

height after de-fluidization was about 1.4 times their initial bed height. It is important to

state that although good results were observed for the jet assisted fluidization at a reduced

nozzle operating pressure of 75 psig, it does not imply that any arbitrary choice of

operating pressure is feasible for processing the powder. This is because the pressure

controls the jetting velocity, and given the size of the nozzle; at very low pressures the

velocity through the orifice would be too small. An alternative view of the behavior of the jet at the different pressures is shown in the jet processing plot. The legend on

■ TiO2 - Blue nozzle-120 psi-1.5lpm-0.025 m/s
□ TiO2 -Blue nozzle-75 psi-1.1 lpm- 0.025 m/s
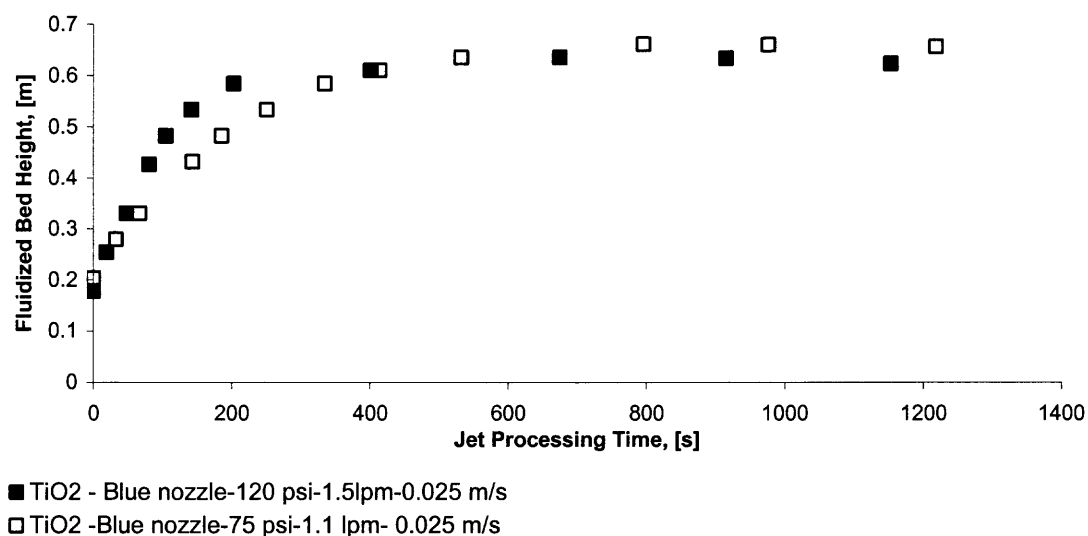
Figure 3.20 Jet processing of TiO$_2$ at 75 and 120 psig

Figure 3.20 should be read as the jet processing of TiO$_2$ using the blue nozzle (254 μm) with gas flow coming in at a pressure of (120 or 75) psig, which translates into a jet flow of (1.5 or 1.1) lpm, and coupled with the primary flow through the column gives a total gas velocity of (0.025) m/s. From the figure, it is seen that the initial kinetics of the 120 psi nozzle was faster than that of the 75 psi within the 1400 seconds window. The 120 psig flow reaches a steady value after approximately 250 seconds but this does not happen with the 75 psi nozzle until after 400 seconds. At the end point, both curves reach approximately the same processed bed height value, which implies that both pressures are capable of processing the mass of powder used in the experiment.

To further test the performance of the nozzle, the mass of powder that was used was increased from 61g to 255g, which is a 4.2 times increase in mass. The result for this experiment is described in Figure 3.21.
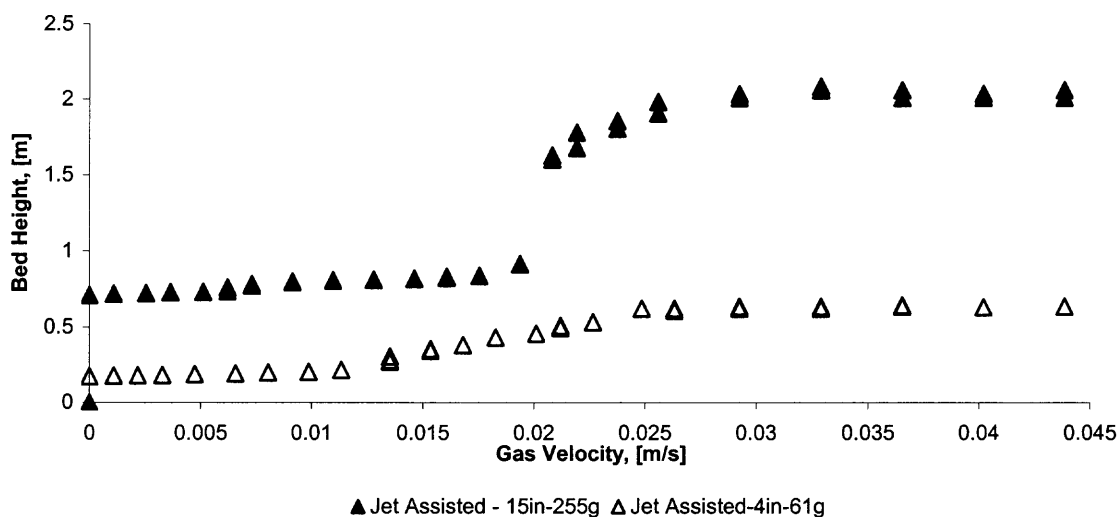
Figure 3.21 Comparison between the jet assisted and conventional fluidization 61 and 255g of TiO_2 at different nozzle distances.

In the experiment utilizing 255g of TiO_2, the nozzle position was shifted from 4 inches above the distributor plate to 15 inches. This was done to further test the impact of the micro nozzle on the fluidization of the powder, because previous experiments showed improved contacting when the nozzle was at the 4 inch position. The result is the fluidization curve depicted in Figure 3.21. It shows that by changing the nozzle position to 15 inches and increasing the mass of the powder by 4.2 times the initial mass of 61g, the maximum bed height attained was 4.4 times its initial bed height of 0.457 m compared to bed height of 5.7 times the initial bed height of 0.114 m achieved when 61g of TiO_2 was used and the orifice of the nozzle was located 4 inches above the distributor plate as indicated by the curve. Also, after, defluidizaton, the final bed height was 0.711 m for the 255 g run, and 0.173 m for the 61 g run. In either case, the performance of the jet assisted fluidization was better than the conventional case, which gave just a 1.3 times increase in bed height due to bubbling.

The effect of multiple nozzles on the behavior of the jet assisted fluidization of TiO$_2$ was also examined. The idea was to increase the total jetting velocity from the nozzle by increasing the number of nozzles. As previously mentioned, the maximum operating pressure (120 psig) creates an upper bound for the jetting velocity and in order to exceed that velocity, the number of nozzles has to be increased. According to Guo et al (2002), the presence of multiple nozzles affects the flow pattern within the fluidized bed, because now you have jets which can either emerge as segregated or coalesced depending on the jetting velocity and the separation distance between the nozzles. A plot of the observations made with regards to the fluidization behavior using the multiple configurations is represented in Figure 3.22.
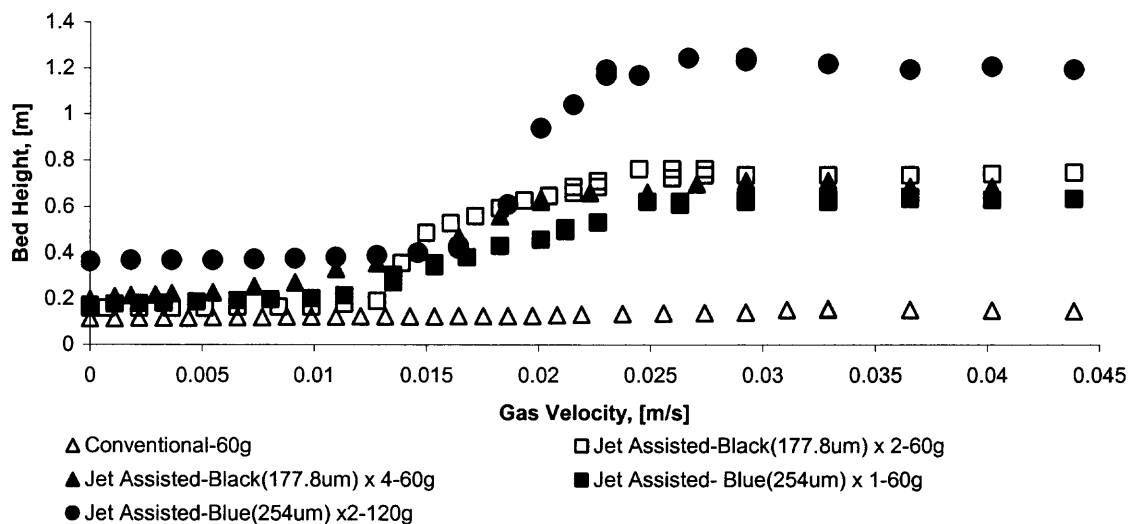
Figure 3.22 Effect of Jet assisted fluidization with multiple nozzles on TiO$_2$.

For the different cases shown in the figure, the experiments were performed at an operating pressure of 120 psig. The figure shows that for all the configuration of multiple nozzles, at a velocity of 0.04 m/s, the bed of TiO$_2$ agglomerates was dispersed about six times its initial bed height, which was much better to the 1.3 times expansion obtained at

the same velocity when the bed was fluidized conventionally. As shown previously in Figure 3.21, the weight of the bed affects the fluidization behavior under the jet assisted mode for TiO_2, and in Figure 3.22, it is reconfirmed. When 120g of TiO_2 were fluidized using two 254 μm (blue) nozzles, the circular points between 0.01 to 0.015 m/s show a delay in the impact of the nozzle on the powder. This is a direct indication of a higher minimum fluidization velocity, and in comparing the bed expansion under different configurations, it is also seen to have a slightly lower bed expansion of about five times the initial bed height. In comparing the general trend of the jet assisted fluidization of TiO_2 (ABF) and R974 (APF), it seen that the bed height vs. gas velocity plot with different amounts of powder matches closer with R974, despite the APF like behavior observed for TiO_2 when it is jet assisted..

3.3.5 Jet Assisted Fluidization of A90

The effect of the micro nozzle jet on the fluidization behavior of Aerosil A90 was also studied. The conventional fluidization behavior of A90 has been classified as ABF by previous researchers. When fluidization of the powder is attempted conventionally, A90 is mostly noted for the electrostatic charge build up which causes powder to stick to the wall and hinders fluidization. Prior to running an experiment the powder is pre-sieved with an 850 μm mesh tray to remove large agglomerates. The key parameters that were varied included nozzle size, nozzle orientation, number of nozzles, mass of powder, and operating pressure. In analyzing the impact of the nozzle on the fluidization behavior, plots comparing the pressure drop and bed expansion against gas velocity, and bed expansion vs. jet processing time were used. By using different nozzle sizes at the same

pressure, the exit jet velocity through each nozzle will be different, and this in turn affects the jet penetration height, momentum dissipation and shearing rate of the nozzle. The typical behavior of agglomerates of A90 under the influence of different nozzle sizes can be seen in Figure 3.23.
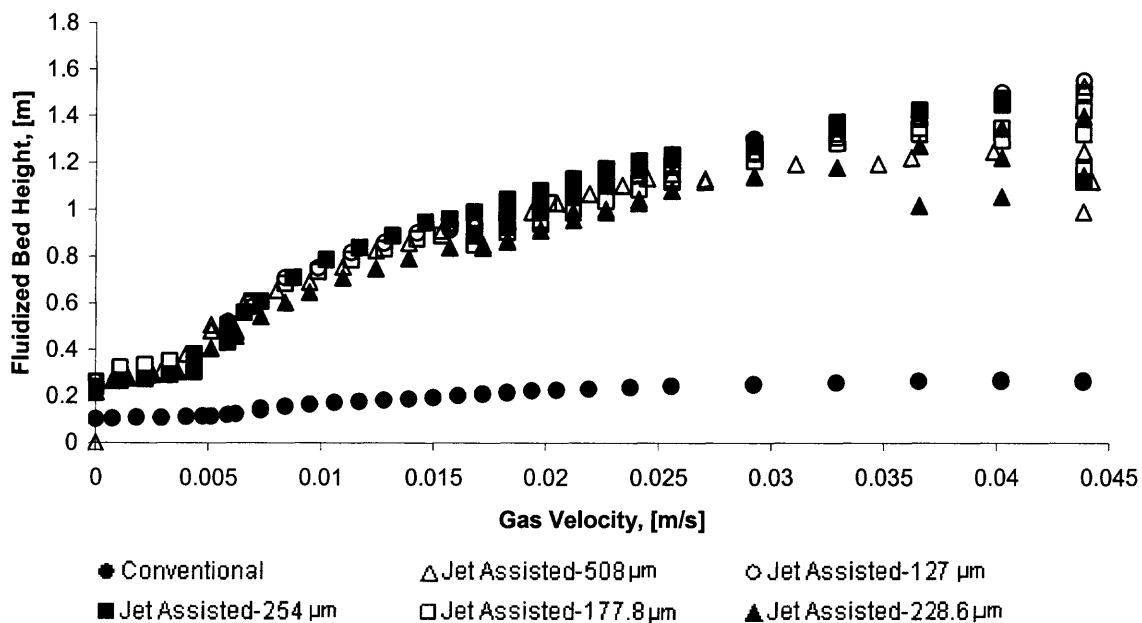
Figure 3.23 Jet assisted fluidization of A90 with nozzles of different sizes.

The figure compares the effect of the different nozzle sizes on the jet assisted fluidization of 18 g of A90. The most notable observation is the huge difference between the expansion of the bed when conventionally fluidized compared to when fluidized with the aid of the micro nozzle jet. For all the nozzles sizes, at a velocity of 0.045 m/s, the expansion of the bed was in the range of 12 to 13 times the initial bed height as compared to the 2.4 times observed when fluidized conventionally. Looking at just the jet assisted fluidization curves, there is a difference in the bed height observed at higher velocities,

which is due to the electrostatic nature of the powder. The electrostatic charge builds up after running the fluid through the fluidized bed for an extended period of time, and this usually causes a decrement in the bed expansion. In cases where the bed falls below an acceptable limit, the nitrogen supply is turned off, and the electrostatic condition is reduced via the use of an electrostatic dissipater. Prior to running the experiment, the wall of the column is cleaned with electrostatic spray. When a noticeable difference is observed, the flow is then resumed and progressively increased until the bed expansion and observations match the values prior to shutting down the flow.

In both the conventional and jet assisted fluidization, bubbling was generally observed at velocities greater than 0.03 m/s, but for jet assisted fluidization, the bubbles were usually less frequent, until a much higher velocity was attained. Upon de-fluidization of the bed, the bed height after jet processing was usually in the range of 2.2 to 2.5 times the initial bed height, which suggested that the bed of agglomerates was changed by the action of the micro nozzle jets. This can also be inferred by looking at the processed powder which appears much fluffier than it was prior to fluidizing with the jet. The response of the pressure drop to the gas velocity for both the conventional and the jet assisted fluidization is shown in Figure 3.24.
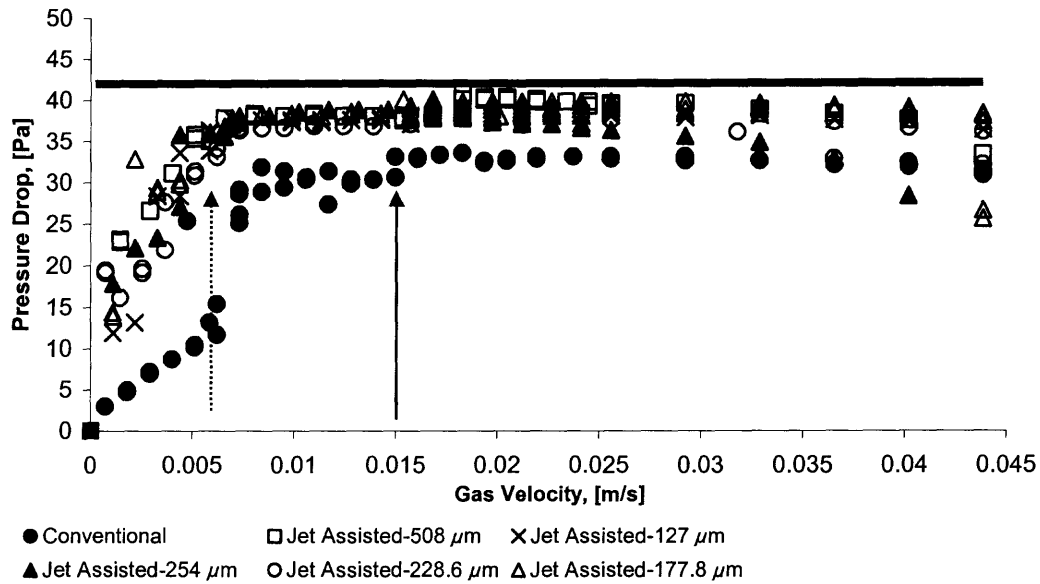
Figure 3.24 Effect of gas velocity on the pressure drop for the fluidization of 18 g of A90 using different nozzles.

From the figure, the corresponding minimum fluidization velocity can be found. Coincidentally, the u_{mf} under the influence of the jet is approximately the same for each of the nozzles tested. In the jet assisted mode, the u_{mf} value is 0.0058m/s, which is less than the conventional fluidization value of 0.015 m/s as shown by the two vertical pointing arrows in the figure. The dotted arrow corresponds to the jet assisted and the solid arrow to the conventional. It is also seen in the plot that under the action of the jet, more A90 is being suspended, and this is represented by the proximity of the pressure drop value to the apparent weight of the particles. At velocities greater than 0.025m/s the, values of the pressure drop for the jet declines, due to the presence of increasing electrostatic conditions in the powder bed, and this generally implies that less powder is been lifted during the jet assisted fluidization..

Also of importance is the effect of nozzle pressure on the fluidization behavior of A90 with jet assistance. To operate at a lower pressure, implies cutting the amount of

work required to process the powder. The effect of the blue nozzle (254 μm) at 120 and

80 psig on the jet assisted fluidization of A90 is described in Figures 3.25 and 3.26
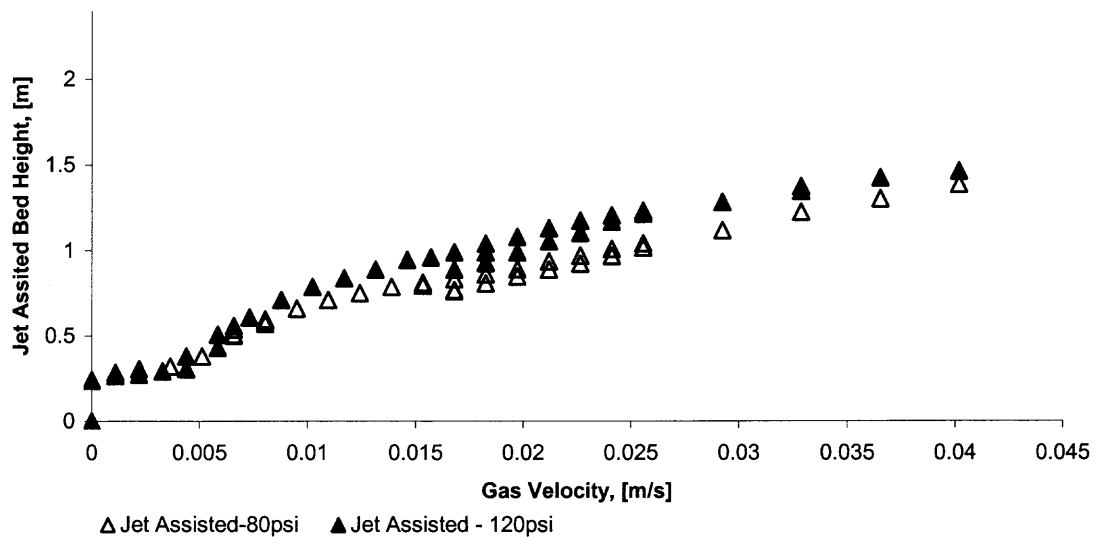
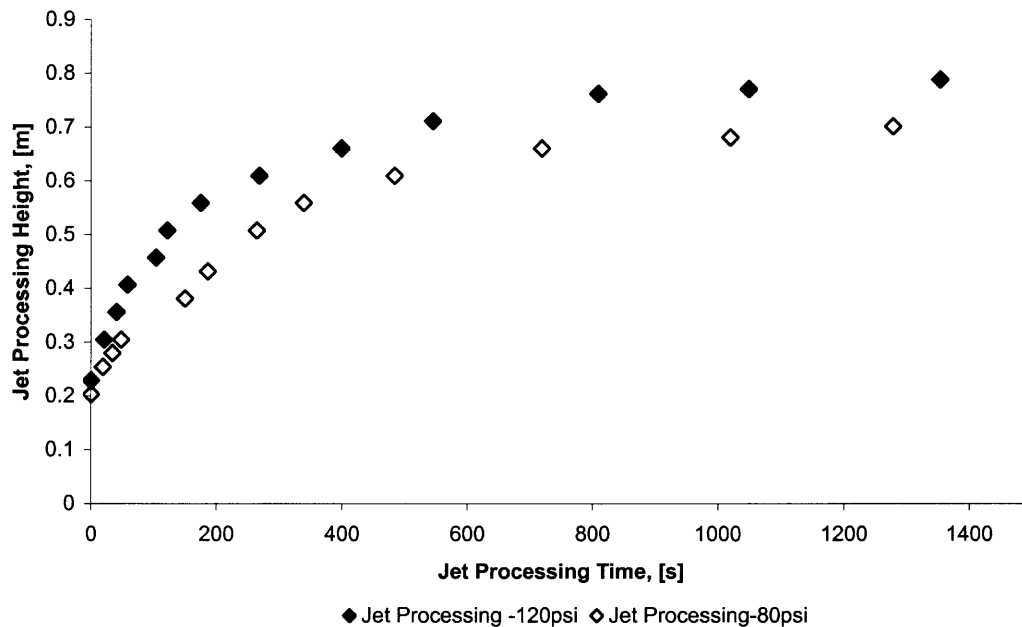**Figure 3.25** Effect of pressure on the fluidization behavior of A90.

Figure 3.26 Effect of pressure on the jet processing of A90.

Figure 3.25 represents the response of A90 to increasing gas velocity during the

jet assisted fluidization with nozzle pressures at 80 and 120 psi, while Figure 3.26

represents the jet processing curve as a function of time for the same A90 agglomerates under 80 and 120 psi. The powder behavior was studied by using the blue nozzle with 254 μm orifice size to process and fluidize 18g of powder sample at 80 and 120 psi. The jet assisted fluidization curves were found to be very similar, with the regards to shape, and behavior. It is clearly seen in both cases that the jet assisted fluidization gives a bed expansion of about 11 times for an initial bed height of about 0.11m at a velocity of 0.04 m/s. Comparing the fluidization behavior at the two pressures, it seen that better expansion is observed when the nozzle's operating pressure is 120 psig.

The effect of pressure on jet processing rate is important, because it represents how much work input is required to process the powder. Furthermore, it becomes useful information when the available fluid source pressure differs from the ones already presented. Figure 3.26 shows that in the 1400 seconds window the jet processing rate at 120 psig was better than the rate at 80 psig. Initially, the kinetics of the 120 psi nozzle is greater, as shown by the steeper curve between 0 and 400 seconds. This trend however, follows through to 1400 seconds. This behavior also supports the difference found in the fluidization curve.

The impact of multiple nozzles was also examined with regards to the jet assisted fluidization of A90 powder. The results are shown in Figure 3.27 and 3.28.
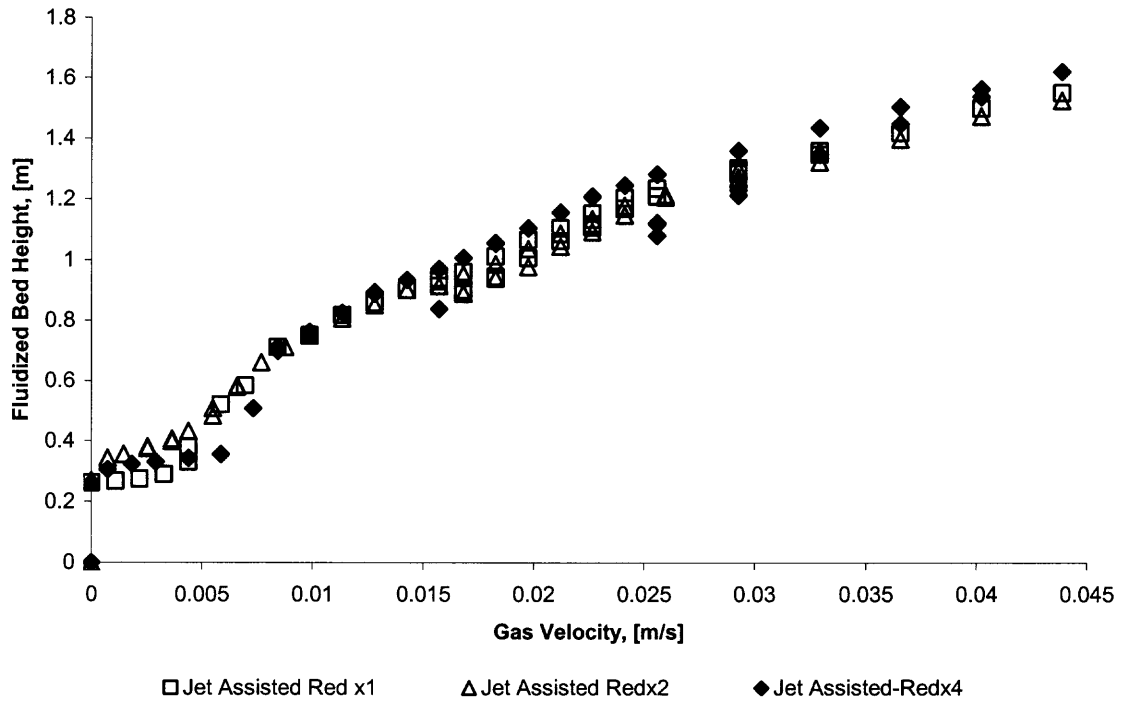
Figure 3.27 Effect of gas velocity on the fluidization behavior of 18 g of A90 when fluidized with multiple nozzles.
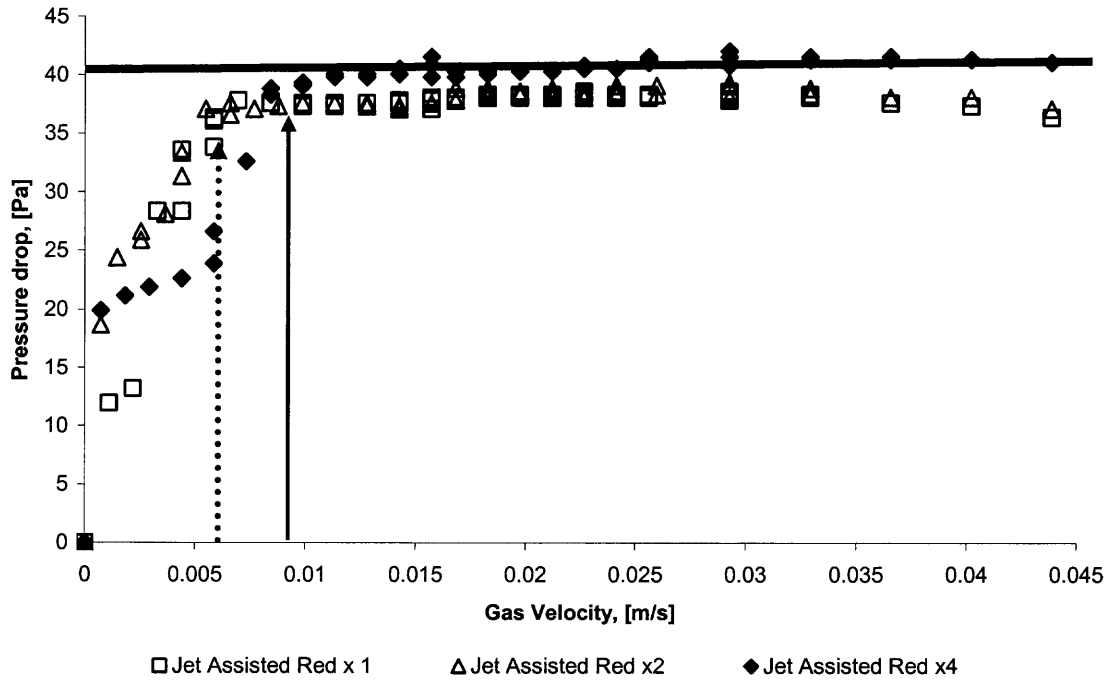
Figure 3.28 Effect of gas velocity on the pressure drop of 18 g of A90 when fluidized with multiple nozzles.

Figure 3.27 shows the effect of gas velocity on the bed height of an 18 g bed of A90 under the influence of multiples nozzles, while Figure 3.28 shows the response of the pressure drop to the increasing gas velocity. In the set of experiments represented in the Figures 3.27 and 3.28, 1, 2 and 4 multiples of the red nozzle (127 μm) were used. It is seen in Figure 3.27, that regardless of the number of nozzles that were used, the bed expansion was still in the order of 13 times the initial bed height at a gas velocity of 0.045 m/s. Upon de-fluidization it was observed that the final bed height was over 2 times the starting bed height. As explained earlier, deviations from the curve were attributed to electrostatic changes in the fluidized bed.

In Figure 3.28 the arrows point to the minimum fluidization velocity which was determined to be 0.006 m/s when 1 and 2 red nozzles were used and 0.008 m/s when 4 red nozzles were used. It can be seen that under the influence of the jet, all the powder is dispersed upon fluidization. This is confirmed by the value of the pressure drop which is approximately equal to the apparent weight of the bed denoted by the solid horizontal line.

Other configurations of nozzles found in literature, are horizontal, upward pointing, and inclined nozzles. With regards to the orientation of the nozzle, the effect of two upward facing nozzles was also investigated, and this effect was compared to using two downward pointing nozzles.

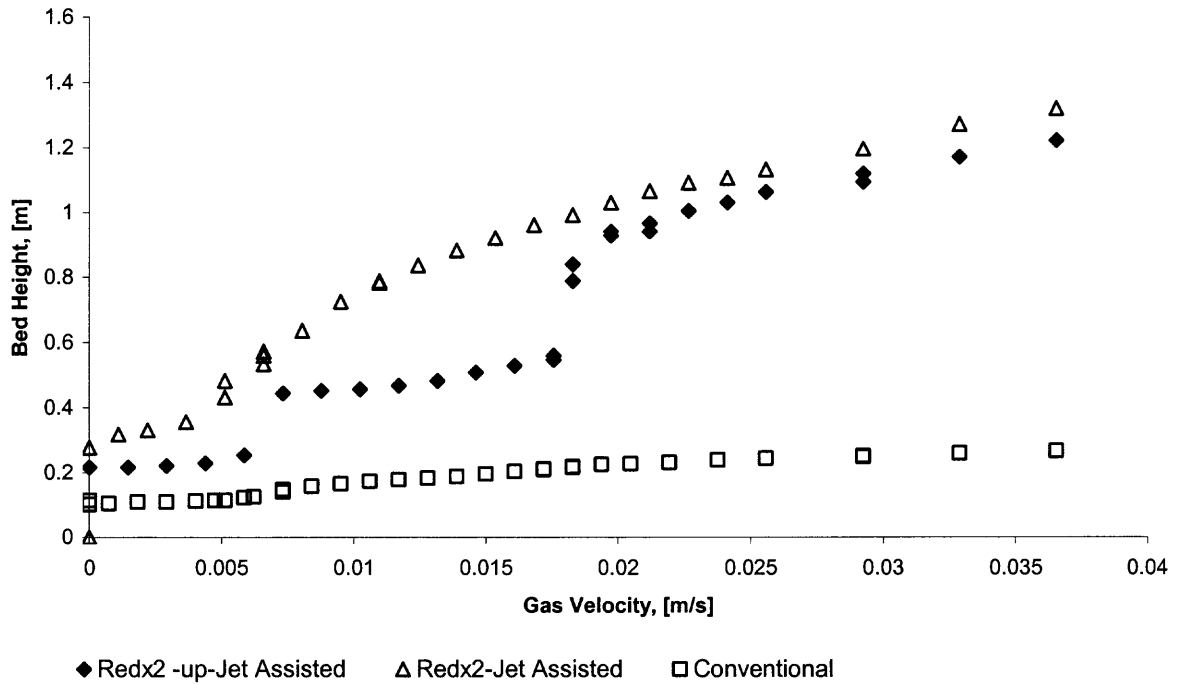**Figure 3.29** Effect of nozzle orientation on the jet assisted fluidization of 18g Aerosil A90.
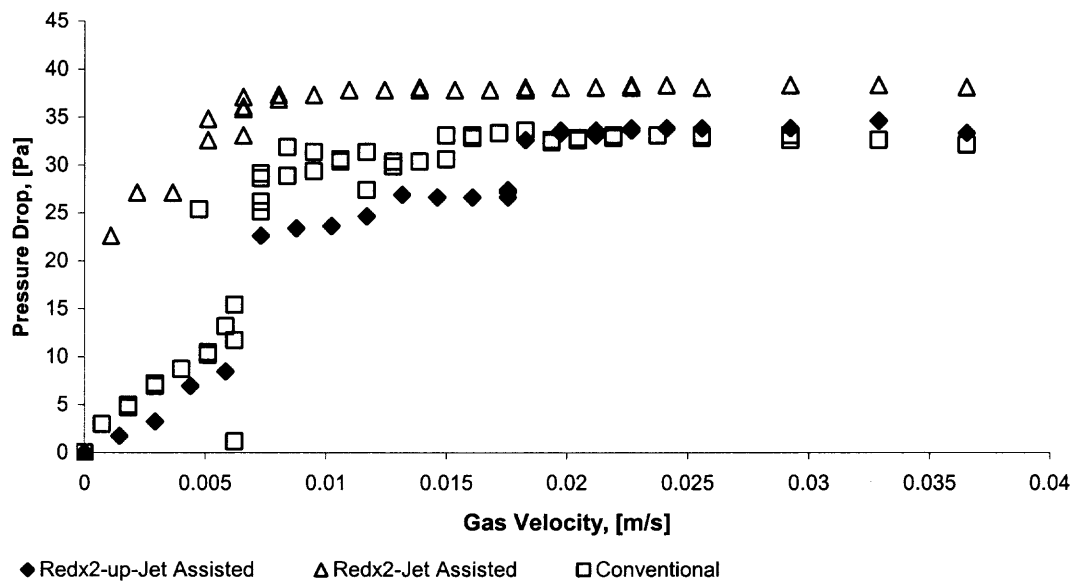

Figure 3.30 Effect of nozzle orientation on pressure drop vs. gas velocity plot for 18g of Aerosil A90.

Figure 3.29 shows the effect of gas velocity on bed height for 2 upward and 2 downward oriented nozzles, and compares their behavior to that of the conventional mode, while Figure 3.30 shows the effect of nozzle orientation on the pressure drop vs. gas velocity plot. Figure 3.29 shows that the jet assisted fluidization curve using the double upward pointing nozzles resembles a step function, which stabilizes after 0.018 m/s. During the experiments, it was visually observed that the upward nozzle was only effective at high primary gas flow rates when there was a significant amount powder above the jet. Also observed was that powder below the nozzle did not circulate into the jetting region above the nozzle. From the figure, it is apparent that the upward nozzle is also able to disperse the powder to about 12 times its initial bed height at a gas velocity of about 0.037 m/s, which is a better result compared to the 2.2 times bed expansion obtained for the conventional fluidization of A90. However, due to the aforementioned observations, the downward orientation showed better fluidization results and is clearly preferred.

With regards to the pressure drop, the upward nozzle's response was also stepwise. From Figure 3.30, the minimum fluidization velocities observed were 0.006 m/s for the jet assisted with the downward orientation, 0.008 m/s for the conventional fluidization and 0.018 m/s for the upward pointing double nozzle. Also observed was that the downward pointing nozzle supported more of the A90 agglomerates compared to the upward pointing nozzles. This is shown by the larger pressure drop values for the downward pointing nozzle after the u_{mf} point compared to the upward nozzles. The use of the upward nozzle also signified that the entirety of the powder in the bed was not fluidized, due to the region of slow moving powder found below the jet.

3.3.6 Jet Assisted Fluidization Coupled with Internal Perforated Plates

Internals, as previously mentioned, are used to enhance the fluidization behavior by improving gas and solid mixing, breaking down bubbles, increasing bubble frequency, facilitating radial distribution of solids and can produce other improvements, depending on the design of the internal (Yang 2003). The internals tested in this work were three different perforated plates, with a distribution of uniform holes on their surface and located 12 inches above the distributor. The effect of the perforated plates on fluidization behavior was investigated using 27 g of Aerosil A90. Figure 3.31 shows the fluidization behavior observed for the jet assisted fluidization of A90 agglomerates using the 3
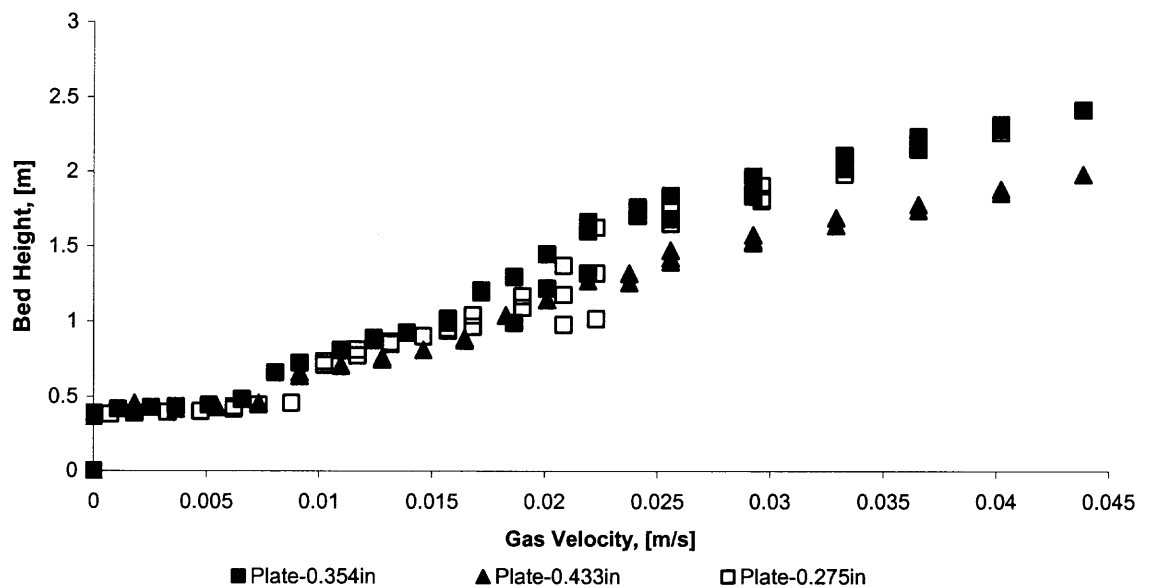

Figure 3.31 Bed height as a function of gas velocity for different internal systems

different perforated plates. Prior to turning on the jet, when the powder was fluidized conventionally through the plate to a certain height above its 12 inches location, the powder constantly separated into two layers, where most of the large agglomerates

remained below the plate and the finer particles rose above it. The layer below the plate acted simply as a packed bed and showed no expansion. The fluid passing through this packed bed region was not uniformly distributed, due to the presence of channels in certain areas, and this eventually contributed to the collapse of the layer of fine particles found above the perforated plate.

In the jet assisted case, the nozzle was located at a 4 inch point above the perforated plate, and its flow coupled with the primary gas flow could be used to maintain a uniform and continuous fluidization above and below the plate. This behavior is represented in Figure 3.31. For all their usefulness, the plates are still obstacles, through which the powder has to pass through or more correctly speed through. It was observed that the powder had a tendency to collapse and separate into layers, when the gas velocity was between 0 to 0.023 m/s, but at velocities greater than 0.03 m/s, the bed was steady and continuous.

In experiments done with the plates, the bed expansions were in the order of 12 to 14 times the initial bed height at a gas velocity of 0.044 m/s. The best results were achieved for the plate with 0.354 inch holes, and bubbles were suppressed when any of the plates were used. The observed minimum fluidization velocities of the nanoparticle agglomerates when the plates were present were found to be higher than the values previously reported for fluidization without a plate as shown in Figure 3.32.

X Plate-0.433in ▲ Plate-0.275in ■ Plate-0.354in
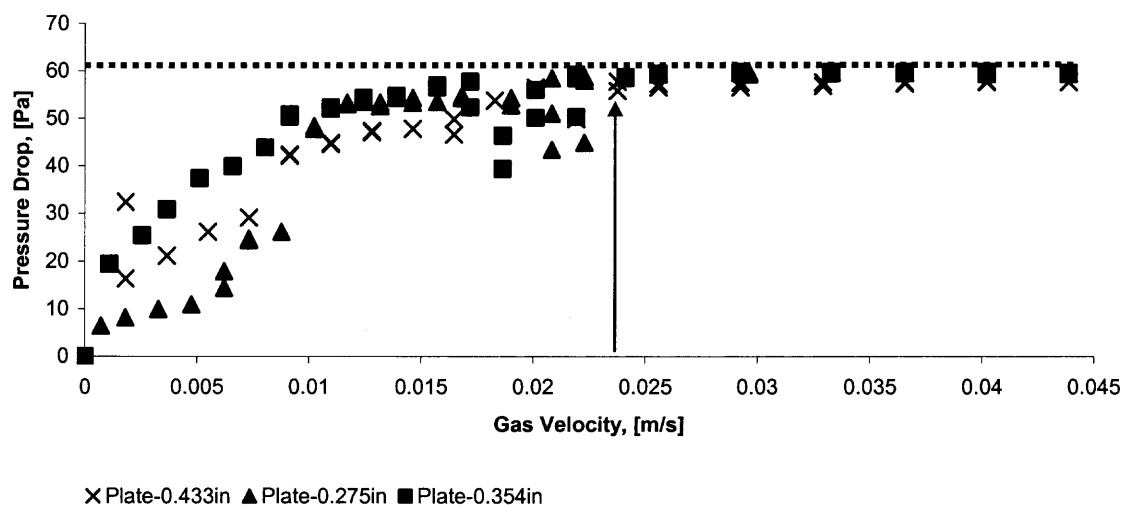
Figure 3.32 Pressure drop as a function of gas velocity for different internal systems.

In the figure, the solid arrow shows the minimum fluidization point. The u_{mf} was approximately 0.023 m/s for all of the plates which is a higher value when compared to 006 m/s (Figure 3.23) obtained when there was no plate present. As mentioned with regards to the bed expansion in Figure 3.31, the bed was not very stable at velocities below 0.23 m/s, and this is corroborated by Figure 3.32. In order for powder to pass through the plate, it has to have sufficient momentum else there will be discontinuity in the fluidization. The required level of momentum is achieved at the u_{mf} point in the plot. After reaching the minimum fluidization point, it is also shown in the figure that approximately all the powder is been suspended. This is indicated by the proximity of the pressure drop values to the apparent weight of the bed.

CHAPTER 4

CONCLUSIONS

The previous chapter has introduced the nanopowders, their properties and their behavior in response to both conventional and jet assisted fluidization. The results section showed in detail the differences observed when agglomerates of nanoparticles are subjected to the jet assisted fluidization which employs a downward facing micro nozzle, as compared to conventional fluidization (without jet assistance). Under the influence of jet, the results show a combination of high bed expansion, total suspension of the bed of particles, reduction of the size of large agglomerates, homogenous fluidization, no bubbling, and a reduction of the minimum fluidization velocity (u_{mf}) for the different powders that were used. In particular, for ABF particles which are known for their poor quality of fluidization, low bed expansion and vigorous bubbling, it was possible to achieve APF type fluidization behavior.

For Aerosil R974, which is a hydrophobic APF powder, the effect of the jet on the fluidization of different amounts (masses) of the powder was explored. The jet assisted fluidization produced a bed expansion as large as 55 times the initial bed height, and total suspension of bed particles, compared to an expansion of only 5 times the initial bed height, and only partial suspension of the powder during conventional fluidization at a gas velocity of 0.04 m/s. The jet also reduced the minimum fluidization velocity, and no bubbling was observed. To further, test the impact of the jet, an unsieved version of the powder was also used. Normally, unsieved R974 shows a bed expansion of only about 1.3 times, but through the action of the jet, a bed expansion as high as 30 times was

observed. Also, in regards to R974, the final value of the bed expansion ratio for the bed of particles was similar for the different masses of powder that were used.

The behavior of Aerosil A200, a hydrophilic nano silica, was also studied. A200 is also classified as an APF powder, but it produces a significant amount of electrostatic charge when fluidized due to triboelectrification which results in a poorer fluidization quality. For both the conventional and jet assisted cases, the bed expansion of A200 was found to be less than that of R974. For example, at a flow rate of 0.04 m/s, A200 expands 11 times under the influence of the jet and 4.5 times when fluidized conventionally, while R974, as mentioned above expands 55 times for the jet assisted mode, and 5 times for conventional fluidization. However, this does not change the fact that the presence of the jet had an impact on the fluidization behavior of the A200 powder. Also, the minimum fluidization velocity for both modes was around 0.006 m/s, but the amount of powder being suspended by the nitrogen gas was larger for the jet assisted fluidization as indicated by the pressure drop plot.

The effect of the jet assisted method on the fluidization of Aeroxide Alumina C, which is an ABF powder, was also studied. During conventional fluidization, it expanded 1.6 times the initial bed height at a gas velocity of 0.05 m/s, but by the action of the micro nozzles, it was possible to expand the powder up to 14 times at the same flow conditions. The jet assisted fluidization also reduced the minimum fluidization velocity of the powder from 0.008 m/s for the conventional case to 0.0055 m/s, and it was also observed that more powder was being suspended when the jet was used as observed from pressure drop measurements.

Another ABF powder, Aeroxide TiO_2 was studied under the conventional and jet assisted fluidization modes. Compared to Aeroxide Alu C, commercial TiO_2 is a much denser nanopowder, and it displays a more typical ABF like fluidization behavior (non homogeneous fluidization, very low bed expansion, and vigorous bubbling. RAW TiO_2 fluidized somewhat better and showed a better bed expansion compared to commercial TiO_2, when fluidized conventionally, and both grades of the powder expanded much better under the influence of the jet. For example at a gas flow rate of 0.04 m/s, a bed expansion of 1.3 times the initial bed height was found for TiO_2, and 1.6 times for the RAW grade, and upon fluidization with a 254 μm nozzle, the bed expansion increased to 6 times for the commercial grade, and 4 times for the process (RAW) grade. It was also found that the minimum fluidization velocity for TiO_2 was 0.01m/s for conventional and 0.015 m/s for jet assisted fluidization. For the RAW grade the minimum fluidization was 0.025 m/s for both the conventional and jet assisted cases. It was also observed that more of the TiO_2 and RAW TiO_2 powder were suspended by the gas phase under the influence of the jet as shown by pressure drop measurements. The most important observation made however, was regarding the quality of fluidization during the jet assisted fluidization, where both TiO_2 powders fluidize as APF type nanopowders.

More work was done with the TiO_2 particles in order to further demonstrate the impact of the jet. The effect of pressure, powder weight, and the number of jetting nozzles on the jet assisted fluidization of TiO_2 particles were studied. With regard to lowering the nozzle pressure, it was found that the fluidization behavior of the powder under the influence of a 254 micron nozzle remained the same when represented in a bed height vs. gas velocity plot. However, extra time was needed for processing the powder

when the upstream pressure was 75 psig as compared to 120 psig processing time. When the mass of the powder was quadrupled, less bed expansion was observed. For example at 0.04 m/s, 61 grams of TiO_2 expanded to 6 times its initial bed height, while for 255 grams of powder, the expansion was 4.4 times the initial bed height.

Lastly, the behavior of Aerosil A90 was studied with both conventional and jet assisted fluidization. A90 is an ABF type powder that also produces a considerable amount of electrostatic charge due to triboelectrification when fluidized. For this powder the effect of nozzle size, pressure, number of nozzles, orientation of nozzles, and the influence of internals on the jet assisted fluidization behavior were investigated. For the different nozzle sizes that were used which ranged from 178 μm to 508 μm, the fluidization behavior was similar, but with shifts in the curves due to electrostatic effects. Despite the use of the electrostatic reducer, electrostatic conditions were still apparent after long fluidization periods with nitrogen. At a gas flow rate of 0.045 m/s the observed bed expansion was approximately 13 times, when only 2.4 times was observed when the powder was fluidized conventionally. The observed minimum fluidization velocity was 0.0073 m/s for the conventional case, and this value was reduced to 0.0058 m/s for the jet assisted fluidization with the different sizes of micro nozzle. Almost total suspension of bed particles was observed during the jet assisted fluidization. At a reduced nozzle pressure, the fluidization behavior was very similar, but again showed a difference in the duration of the processing time that was required. This experiment was done at 120 and 80 psig with the 254 μm nozzle. When multiples (1, 2, and 4) of the 127 μm nozzle were used, only very small differences in the bed expansion were observed compared to a single nozzle, and the bed expansion was about 13 times the initial bed height. Also a

complete suspension of the powder in the bed was observed based on the pressure drop measurements whether 1, 2 or 4 nozzles were used.

In changing the orientation of two downward pointing 127 um nozzle to the upward pointing configuration, unsteadiness, and bubbling was observed, except at high primary flow rates. As previously mentioned, this was because the powder below the nozzle did not circulate to the region above it. The plots for both the bed height and pressure drop as functions of the gas velocity for the upward nozzle are akin to step plots, in which they do not achieve the potential of the downward pointing nozzle until more of the powder has been pushed above the nozzle by the primary flow. In terms of the amount of powder suspended, the downward nozzle was also found to be better.

The use of different perforated plates (with different size orifices) as an internal acting within the system to aid circulation of the powder and the gas and to reduce bubbling was also examined. When the powder was fluidized using just the primary flow, the powder separated into two layers. This was because, the plate acted as an obstruction to the normal flow and the primary flow alone could not supply sufficient momentum to accelerate the particles through the orifices of the plate,, but with jet assistance this was possible..

In summary, the major conclusion of this dissertation is that a high pressure downward facing micro jet will greatly improve the quality of fluidization of both APF and ABF type nanoparticles. For APF nanoparticles, bed expansion, and therefore dispersion of the agglomerates, is increased resulting in smaller and fluffier agglomerates. For ABF nanoparticles, which are very difficult to fluidize conventionally without assistance, the jet processing will actually convert them to APF like behavior,

showing a much better fluidization quality, a larger bed expansion, a reduction in the minimum fluidization velocity and very little, if any, bubbling. This is very advantageous since a high minimum fluidization velocity requires more pumping energy and leads to elutriation of particles, and bubbles result in severe gas bypassing leading to poorer utilization of the gas if, for example, it used as a reactant in a gas particle chemical reaction.

Even though the experiments presented in this dissertation have shown that the jet assisted fluidization mode has a huge impact on the fluidization behavior of the nanoparticle agglomerates that were studied, more work is clearly needed. Future studies should focus on developing a theoretical model to predict the size and apparent density of the nanoagglomerates when assisted with the micro jets, measuring jet parameters such as jet breakup length, radial and axial gas velocity profiles near the jet, and the effect of the jets in larger diameter fluidization columns. A predictive model and computer simulation of the jet assisted fluidization is also needed to help in scaling up the process so that it can be applied in the real, process-sized, fluidized bed nanoparticle reactors used in industry.

REFERENCES

Behie, L A., Bergougnou, M A., Baker, C G J., & Bulani, W. Jet momentum dissipation at a grid of large gas fluidized bed. (1970) <u>The Canadian Journal of Chemical Engineering, 48</u>, 58-161.

Blake, T R., Webb, H., & Sunderland, P B. (1990). The non-dimensionalization of equations describing fluidization with application to the correlation of jet penetration height. <u>Chemical Engineering Science, 45</u>, 365-371.

Choi, J., Kim, J., & Kim, S. (1997). Effect of secondary gas injection on the particle entrainment rate in a gas fluidized bed. Powder Technology, 90, 227-233.

Chyang, C S., Chang, C H., & Chang J H. (1997). Gas discharge modes at a single horizontal nozzle in a two-dimensional fluidized bed. <u>Powder Technology, 90</u>, 71-77.

Cleaver, J., Ghadir, M., Tuponogov, V., Yates, J., & Cheesman, D. (1995). Measurement of Jet Angles in fluidized beds. <u>Powder Technology, 85</u>, 221-226.

De Young, D. S., (2004). Theory of Jet Dissipation. Xray and Radio Connections, Santa Fe NM, February 2004, (7.1).

Giblilaro, L. G., (2001). Fluidization Dynamics. Butterworth Heinemann.

Gupta, C. K., & Gupta, C. K., & Sathiyamoorthy, D. (1999). <u>Fluid Bed Technology in Materials Processing</u>. New York: CRC Press LLC., 1-5.

Guo, Q., Yue, G., Zhang, J., & Liu, Z. (2001a).Hydrodynamic Characteristics of a two dimensional jetting fluidized bed with binary mixtures. <u>Chemical Engineering Science, 56</u>, 4685-4694.

Guo, Q., Tang, Z., Yue, G. (2001b). Flow Pattern Transition in a Large Jetting Fluidized Bed with Double Nozzles. <u>AICHE, 47:6</u>, 1309-1317.

Guo, Q., Zhang, J., Werther, J. (2003). Jetting transition velocity in a jetting fluidized with two nozzles. <u>Chemical Engineering Scinece, 92</u>, 63-67.

Guo, Q., Li, Y., Wang, M., Shen, W., & Yang C. (2006) Fluidization characteristics of SiO2 nanoparticles in an acoustic fluidized bed. <u>Chemical. Engineering. Technology, 29</u>, 78-86.

Hakim, F., Portman, J.L., Casper, M.D., & Weimer, A.W. (2005). Aggregation behavior of nanoparticles in fluidized beds. <u>Powder Technology, 160</u>,149-160.

Hong, R Y., Li, H. Z., Cheng, M Y., & Zhang, J Y. (1996). Numerical simulation and verification of gas-solid jet fluidized bed. Powder Technology, 87, 73-81.

Hong, R., Li, H., Wang, Y., (1997). Studies on the inclined jet penetration length in a gas-solid fluidized bed. Powder Technology, 92, 205-212.

Hong, R Y., Guo, Q., J, Luo., G, H., Zhang, J Y., & Ding J.(2003). On the jet penetration height in fluidized beds with two vertical jets. Powder Technology, 133, 216-227.

Hong, R., Ding, J., & Li H. (2005). Fluidization of fine powders in fluidized beds with an upward or a downward air jet. China Particuology, 3(3), 181-186.

Jang, H.D. (2001). Experimental study of synthesis of silica nanoparticles by a bench scale diffusion flame reactor. Powder Technology, 119, 102-108.

Jin Y., Yu, Z. Q., Zhang, L., Shen, J. Z., Wang, Z. W., (1982). Pagoda shaped internal baffles for fluidized bed reactors. Intern Chem Eng, 22(2), 269-279.

Kunii, D., Levenspiel, O. (1991). Fluidization Engineering. Elsevier Science and Technology Books.

Levy, E.K., Celeste, B. (2006). Combined effects of mechanical and acoustic vibrations on fluidization of cohesive powders. Powder Technology, 163, 41-50.

Nam, C., Pfeffer, R., Sundaresan, S., & Dave, R. (2004).Aerated Vibrofluidization of Silica nanoparticles. AICHE, 50, 8 1776-1785.

Quevedo J., Pfeffer, R., Dave, R., Shen, Y., Nakamura, H., & Watano, S. (2006). Fluidization of Nanoagglomerates in a Rotating Fluidized Bed. AICHE, 52:7, 2401-2412.

Quevedo J. (2004). Fluidization of agglomerates of nanoparticles under different force fields. NJIT Thesis.

Rowe, P N., MacGillivray, H J., & Cheesman D J. (1979). Gas discharge from an orifice into a gas fluidized bed. Transactions of the Institution of Chemical Engineering, 57, 194-199.

Shen, Z., Briens, C L., & Bergnougnou, M A. (1990). Study of a downward Grid jet in large two dimensional gas fluidized Bed. Powder Technology, 62, 227-234.

Start, J. W., Pratsinis, S. E. (2002). Aerosol flame reactor for manufacture of nanoparticles. Powder Technology, 126, 103-108.

Tadashi, F., Golman, B., & Shinohara, K. (2006). Batch grinding kinetics of Ethenzamide particles by fluidized bed jet milling. International Journal of Pharmaceutics, 311, 89-96.

Tasirin, S M., Geldart, D. (1999). Experimental investigation on fluidized bed jet grinding. Powder Technology, 105, 337-341.

Vaccaro, S. (1997a). Analysis of the variables controlling gas jet expansion angles in fluidized beds. Powder Technology, 92, 213-222.

Vaccaro, S., Musmarra, D., & Petrecca, M. (1997b). A technique for measurement of the jet penetration height in beds by Pressure Signal Analysis Powder Technology, 92, 223-231.

Wang, X.S., Palero, V., Soria, J., & Rhodes, M.J. (2006), Laser-based planar imaging of nano-particle fluidization: Part I-determination of aggregate size and shape. Chemical Engineering Science, 61, 5476-5486.

Werther, J., Xi, W. (1993) Jet attrition of catalyst particles in gas fluidized beds. Powder Technology, 76, 39-46.

Xuereb, C., Laguerie, C., & Baron, T. (1991). Etude du comportement de jets continus horizontaux ou inclines introduits dans un lit fluidise par un gaz. I: Morphologie des jets. Powder Technology. 67, 43-56.

Yang, W C., (1998). Comparison of jetting phenomena in 30-cm and 3-m diameter semicircular fluidized beds. Powder Technology, 100, 147-160.

Yang, W C., (2003). Handbook of Fluidization and Fluid-Particle Systems. Marcel Decker, Inc.

Yao, W., Guangsheng, G., Fei, .W, & Jun, W. (2002). Fluidization and agglomerate structure of SiO2 nanoparticles. Powder Technology, 124, 152-159.

Yu, Q., Dave, R., Zhu, C., Quevedo, J., & Pfeffer, R. (2005). Enhanced Fluidization of Nanoparticle in an Oscillating Magnetic Field. AICHE, 51:7, 1971-1979.

Zhong, W., Zhang, M. (2005). Jet penetration depth in a two-dimensional spout-fluid bed. Chemical Engineering Science, 60, 315-327.

Zhu, C., Yu, Q., Pfeffer, R., & Dave, R. (2005). Gas Fluidization Characteristics of Nanoparticle Agglomerates. AICHE, 51, 426-439.

Zhu, C., Liu, G., Yu, Q., Pfeffer, R., Dave, R., & Nam, C. (2004). Sound assisted fluidization of nanoparticle agglomerates. Powder Technology, 141, 119-123.